https://doi.org/10.1093/plcell/koac192 THE PLANT CELL 2022: 34: 3961–3982

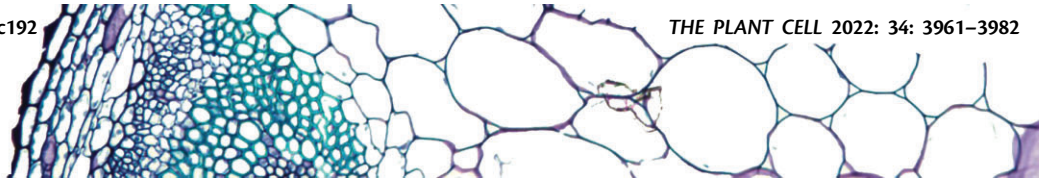

Research Article

AP1/2β-mediated exocytosis of tapetum-specific transporters is required for pollen development in *Arabidopsis thaliana*

Chan Liu [1], Zhimin Li [1], Dan Tian [1], Mei Xu [1], Jianwei Pan [1,†], Haijun Wu [1,*], Chao Wang [1,2,*] and Marisa S. Otegui [3,*]

1 Ministry of Education Key Laboratory of Cell Activities and Stress Adaptations, School of Life Sciences, Lanzhou University, Lanzhou 730000, China
2 College of Life Sciences, Shaoxing University, Shaoxing 312000, China
3 Department of Botany and Center for Quantitative Cell Imaging, University of Wisconsin-Madison, Madison, Wisconsin 53706, USA

*Authors for correspondence: otegui@wisc.edu (M.S.O.); wangc@lzu.edu.cn (C.W.); wuhj@lzu.edu.cn (H.W.)
†Deceased

C.L., M.S.O., J.P., C.W., and H.W. conceived the study and designed the research. C.L., Z.L., D.T., and M.X. carried out the experiments. C.L., M.S.O., C.W., and H.W. analyzed the data. C.L. and M.S.O. wrote the manuscript. All authors revised the manuscript.
The author responsible for distribution of materials integral to the findings presented in this article in accordance with the policy described in the Instructions for Authors (https://academic.oup.com/plcell) is: Chao Wang (wangc@lzu.edu.cn).

Abstract

AP-1 and AP-2 adaptor protein (AP) complexes mediate clathrin-dependent trafficking at the *trans*-Golgi network (TGN) and the plasma membrane, respectively. Whereas AP-1 is required for trafficking to plasma membrane and vacuoles, AP-2 mediates endocytosis. These AP complexes consist of four subunits (adaptins): two large subunits (β1 and γ for AP-1 and β2 and α for AP-2), a medium subunit μ, and a small subunit σ. In general, adaptins are unique to each AP complex, with the exception of β subunits that are shared by AP-1 and AP-2 in some invertebrates. Here, we show that the two putative *Arabidopsis thaliana* AP1/2β adaptins co-assemble with both AP-1 and AP-2 subunits and regulate exocytosis and endocytosis in root cells, consistent with their dual localization at the TGN and plasma membrane. Deletion of both β adaptins is lethal in plants. We identified a critical role of β adaptins in pollen wall formation and reproduction, involving the regulation of membrane trafficking in the tapetum and pollen germination. In tapetal cells, β adaptins localize almost exclusively to the TGN and mediate exocytosis of the plasma membrane transporters such as ATP-binding cassette (ABC)G9 and ABCG16. This study highlights the essential role of AP1/2β adaptins in plants and their specialized roles in specific cell types.

Introduction

Vesicle-mediated trafficking facilitates the exchange of proteins, lipids, and other macromolecules between donor and acceptor organelles in the endomembrane system of eukaryotic cells. Formation of vesicles at donor membranes typically requires cargo adaptor protein (AP) complexes to recruit cargo proteins and other factors, such as coat proteins, required for membrane deformation, into a nascent vesicle bud. Among these cargo adaptors, there are five AP complexes (AP-1 to AP-5) that have similar subunit (also called adaptins) composition: two large subunits containing long and flexible linkers attached to "ear" domains (β1 and γ for AP-1, β2, and α for AP-2), one medium subunit (μ), and one small subunit (σ) (Boehm and Bonifacino,

Received March 02, 2022. Accepted June 21, 2022. Advance access publication June 29, 2022

IN A NUTSHELL

Background: Adaptor protein (AP) complexes are critical for the recruitment of cargo proteins during vesicle trafficking. AP-1 and AP-2 mediate clathrin-dependent trafficking at the *trans*-Golgi network (TGN) and the plasma membrane, respectively. Whereas AP-1 regulates trafficking to the plasma membrane (exocytosis) and vacuole, AP-2 mediates endocytosis. These AP complexes consist of four subunits (adaptins): two large subunits (β1 and γ for AP-1, β2, and α for AP-2), a medium subunit μ, and a small subunit σ. The general roles of some AP-1 and AP-2 adaptins in vegetative and reproductive development have been characterized in plants. However, the function of the large β subunits and whether they are shared by the two AP-1 and AP-2 complexes in plants is currently unknown.

Questions: Are β adaptins shared by AP-1 and AP-2 complexes in *Arabidopsis thaliana*? What function do they play in plant development?

Findings: We found that the two putative Arabidopsis AP1/2β adaptins co-assemble with both AP-1 and AP-2 subunits and regulate exocytosis and endocytosis in root cells, consistent with their dual localization to the TGN and the plasma membrane. However, in tapetal cells of developing anthers, AP1/2β adaptins localize almost exclusively to TGN. Mutations in AP1/2β adaptins result in collapsed pollen grains with abnormal walls and reduced pollen germination due to impaired exocytosis of the tapetum-specific plasma membrane transporters ABCG9 and ABCG16, highlighting the essential role of AP1/2β adaptins in plants and their specialized roles in specific cell types.

Next steps: We will investigate the mechanism by which AP1/2β adaptins recognize cargo proteins and their role in female gametophyte and embryonic development.

2001). AP-1 and AP-2, the AP complexes first characterized, physically linked transmembrane protein cargo to clathrin coats at the *trans*-Golgi network (TGN) and plasma membrane, respectively. AP-1 and AP-2 are recruited to membranes by binding specific phosphoinositides and/or small GTPases, which result in a conformational change that allows the AP complexes to bind motifs on the cytoplasmic domains of membrane protein cargo and recruit clathrin for coat assembly and membrane deformation (Lee et al., 2008; Kelly et al., 2014; Smith et al., 2021).

The capability of AP-1 and AP-2 to associate with multiple proteins during clathrin-mediated vesiculation depends on the coordinated binding activities of the four constituting adaptins. Cargo recruitment is mediated by one or more subunits. For example, the μ subunit binds tyrosine motifs on the cargo proteins (Ohno et al., 1995, 1996, 1998), whereas a hemicomplex of the α and σ subunit selects cargo by binding their dileucine motifs (Janvier et al., 2003; Doray et al., 2007). The ears and linkers of the large β subunit bind clathrin and clathrin-accessory proteins (Shih et al., 1995; Wang et al., 1995; Mishra et al., 2004; Kovtun et al., 2020; Paraan et al., 2020; Smith et al., 2021; Mehrani and Stagg, 2022). In addition, the mammalian β1 subunit has been reported to bind a dileucine motif on cargo proteins as well (Rapoport et al., 1998), making β a uniquely versatile adaptin. In general, adaptins are not shared by different AP complexes, with the exception of some invertebrate β1/2 hydrid proteins (Boehm and Bonifacino, 2001).

Arabidopsis thaliana AP-1 localizes to a sub-domain of the TGN and regulates trafficking to the plasma membrane (exocytosis) and to the vacuole (Park et al., 2013; Wang et al., 2013b, 2014; Heinze et al., 2020; Shimizu et al., 2021), whereas AP-2 localizes to the plasma membrane and plays a role in clathrin-mediated endocytosis (Di Rubbo et al., 2013; Yoshinari et al., 2019; Liu et al., 2020). Both AP-1 and AP-2 complexes are important for plant development as demonstrated by the analysis of Arabidopsis mutants for different AP-1 and AP-2 subunits. Consistent with the role of AP-1 in post-TGN trafficking to plasma membrane and vacuole, AP1γ (large subunit encoded by AP1γ1 and AP1γ2) is required for synergid vacuolar acidification degeneration during fertilization and for proper vacuolar remodeling during pollen formation (Feng et al., 2017; Wang et al., 2017); the two isoforms of AP1μ (AP1μ1 and AP1μ2; medium subunit) act partially redundantly in cell plate assembly during cytokinesis, vacuolar trafficking, pollen, and ovule development, and seed coat mucilage secretion (Happel et al., 2004; Park et al., 2013; Teh et al., 2013; Wang et al., 2016; Shimada et al., 2018). The small subunit AP1σ (AP1σ1 and AP1σ2) regulates pollen wall formation by promoting both the secretion of sporopollenin synthase acyl-CoA SYNTHETASE 5 and LIPID TRANSFER PROTEINs from the tapetum into the anther locule and the plasma membrane localization of the sugar transporter RUPTURED POLLEN GRAIN 1 in microspores (Xu et al., 2022). Supporting a conserved role in endocytosis, Arabidopsis AP2μ mediates the internalization of the auxin efflux carrier PIN-FORMED 2 (PIN2) (Kim et al., 2013) and the plasma membrane brassinosteroid receptor BRASSINOSTEROID INSENTIVE 1 (Di Rubbo et al., 2013; Liu et al., 2020), and is required for proper plant growth, stamen filament elongation, anther dehiscence, pollen formation, and pollen tube growth (Kim et al., 2013; Yamaoka et al.,

2013); the two isoforms of AP2α (AP2α1 and AP2α2; large subunit) are required for root growth (Di Rubbo et al., 2013), whereas AP2σ (small subunit) is important for maintaining polar localization of PIN1 during embryogenesis and plant growth (Fan et al., 2013). However, there is very limited information about the role of the large AP-1 and AP-2 β subunits in plants. Arabidopsis contains two genes encoding putative AP1/2β subunits with hybrid features of both mammalian β1 and β2, but whether these adaptins are required for the function of AP-1 and AP-2 is unclear.

Here, we show that the two Arabidopsis AP1/2β adaptins interact with both AP-1 and AP-2 subunits, consistent with the localization at the TGN and plasma membrane in root cells. The deletion of both β adaptins is lethal in plants. By analyzing mutants with at least one wild-type (WT) copy for either β adaptin gene, we identified a critical role of AP1/2β adaptins in tapetal function and pollen development by regulating exocytosis of plasma membrane transporters required for pollen wall assembly. Thus, this study shows the essential role of AP1/2β adaptins in plants and the versatility of their specialized roles in specific cell types.

Results

Arabidopsis AP1/2β1 and AP1/2β2 are shared by AP-1 and AP-2

The *A. thaliana* genome encodes two putative AP1/2β adaptins, AP1/2β1 and AP1/2β2 (hereafter referred to as β1 and β2, respectively). The amino acid sequences of Arabidopsis β1 and β2 are 93% identical (Supplemental Figure S1, A and B; Supplemental Data Set 1) and have predicted alpha_adaptinC2 and B2-adapt-app_C domains, similar to their animal counterparts (Supplemental Figure S1A).

Whereas mammals typically employ two different β adaptins for the assembly of AP-1 and AP-2, *Drosophila melanogaster* and *Caenorhabditis elegans* have only one shared β1/2 adaptin for both AP complexes. Based on their high amino acid sequence similarity, Arabidopsis β1 and β2 have been suggested to associate with both AP-1 and AP-2 (Boehm and Bonifacino, 2001; Bassham et al., 2008; Yamaoka et al., 2013; Heinze et al., 2020). To determine the molecular interactions of β1 and β2 with other AP and trafficking components, we expressed both adaptins fused to the yellow fluorescent protein (YFP) under the control of their endogenous promoters (*Proβ1:β1-YFP* and *Proβ2:β2-YFP*), and performed immunoprecipitation (IP) from 10-day-old seedling protein extracts using anti-GFP (green fluorescent protein) antibodies followed by tandem mass spectrometry (MS). As control, we performed an IP under similar conditions but using transgenic plants expressing GFP under a constitutive promoter (*Pro35S:GFP*). Input protein extracts and co-IPs from three biological replicates were then trypsinized and analyzed using spectral area-based label-free quantification (LFQ) to measure protein abundance. We calculated the ratio of protein abundance between co-IPs and inputs for each sample to identify significantly enriched proteins ($P < 0.05$) in co-IPs and used the GFP co-IP control to discard unspecific interactions (Figure 1A, see "Materials and methods"). We identified 83 and 41 proteins in the β1-YFP and β2-YFP co-IPs, respectively (Supplemental Tables S1 and S2). Gene ontology (GO) analysis revealed a >100-fold enrichment in "receptor-mediated endocytosis" for both co-IPs (Figure 1B; Supplemental Tables S3 and S4). We identified all the subunits of Arabidopsis AP-1 (AP1γ1, AP1γ2, AP1μ1, AP1μ2, AP1σ1, and AP1σ2) and AP-2 (AP2α1, AP2α2, AP2μ, and AP2σ) in the β1-YFP and β2-YFP co-immunoprecipitates (Supplemental Tables S1 and S2), suggesting that the two β adaptins are able to co-assemble with subunits of both complexes. To confirm these results, we tested the ability of β1 and β2 to associate with the other AP-1 and AP-2 adaptins by a split YFP-based bimolecular fluorescence complementation (BiFC) assay. Here, we detected robust YFP reconstitution when either β1 or β2 fused to the N-terminal domain of YFP (YN) were co-expressed with AP1γ1, AP1μ1, AP1σ2 (AP-1 complex), AP2α1, AP2μ, and AP2σ (AP-2 complex) fused to the YFP C-terminal fragment (YC; Figure 1, D and E). To test whether β1 and β2 are able to assemble into other AP complexes, we performed additional BiFC assays with the large (δ for AP-3 and ε for AP-4), medium (μ), and small (σ) subunits of AP-3 and AP-4 (Supplemental Figure S2). The β1 and β2 adaptins interacted strongly with AP3μ and AP4μ, but not with the other AP-3 and AP-4 subunits, suggesting that β1 and β2 do not form stable complexes with AP-3 and AP-4 subunits. Together with the fact that AP-3 and AP-4 subunits were not detected among the proteins specifically enriched in the β1 and β2 co-IPs (Supplemental Tables S1 and S2), we concluded that β1 and β2 only form stable complexes with AP-1 and AP-2 subunits.

Interestingly, although we detected all the AP-1 and AP-2 subunits present in the co-IPs of both β1-YFP and β2-YFP, there was a relatively large proportion of unique proteins in each co-IP (58/83 for β1-YFP and 16/41 for β2-YFP; Figure 1A; Supplemental Tables S1 and S2), suggesting that the two proteins may not be completely redundant in function.

β1 and *β2* adaptins are broadly expressed and encode plasma membrane/TGN-localized proteins

Based on RT-qPCR (real time quantitative PCR) transcript quantification, *β1* and *β2* are broadly expressed in both vegetative and reproductive tissues; however, whereas *β1* is most highly expressed in floral buds and flowers, *β2* transcripts are most abundant in siliques (Figure 2A). To further analyze the expression patterns of *β1* and *β2*, we expressed the beta-glucuronidase (GUS) coding sequence under the control of either the *β1* or *β2* promoter regions. The strongest GUS staining signal was detected in anthers, pollen grains, and pollen tubes of plants expressing *Proβ1:GUS* and in developing embryos (late globular to torpedo stages) of *Proβ2:GUS* transgenic lines (Figure 2B; Supplemental Figure S3).

To better understand the expression patterns of both genes in anthers and pollen, we analyzed cross-sections of

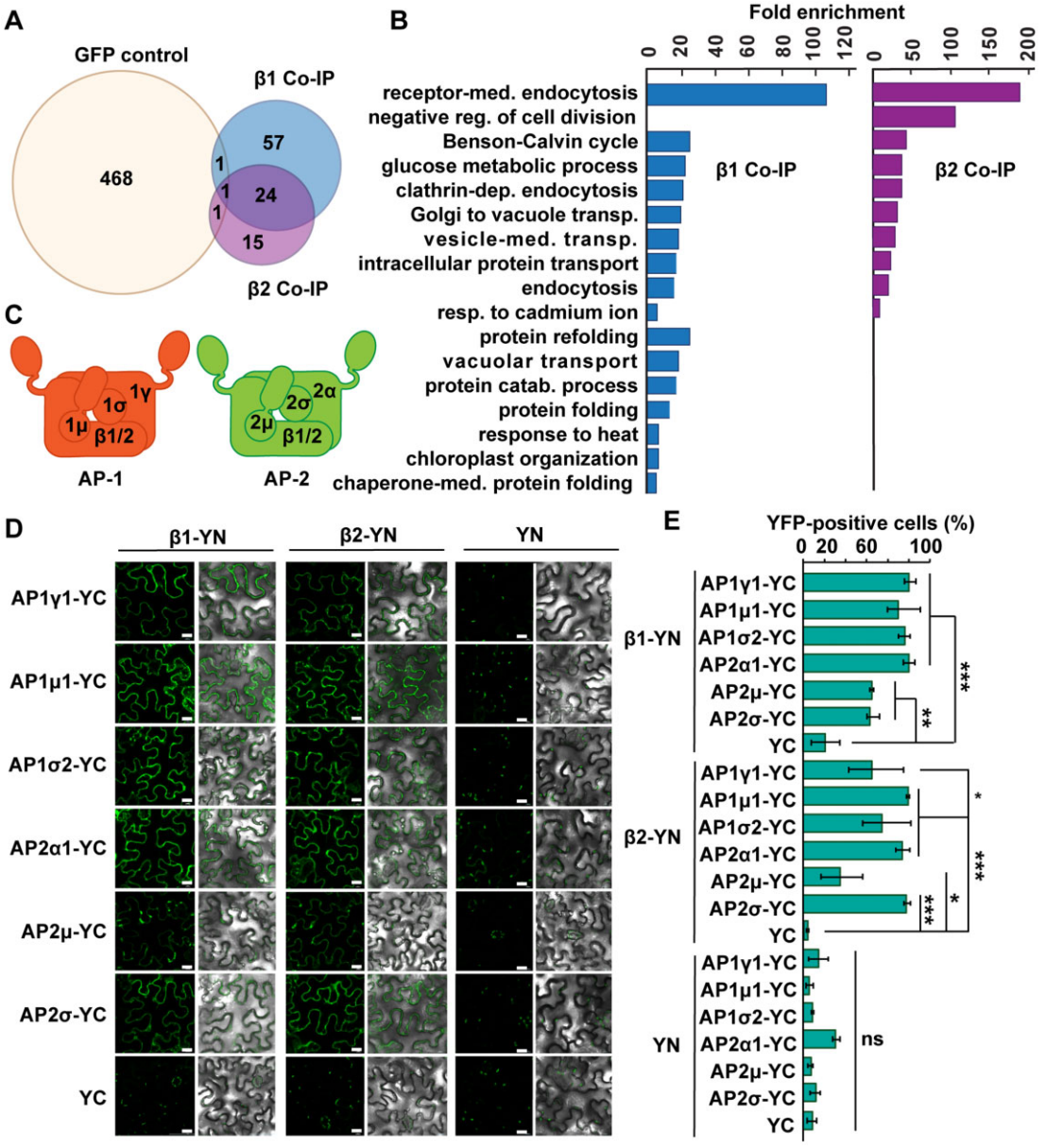

Figure 1 Protein interaction of Arabidopsis β1 and β2. A, Venn diagram showing the common and unique proteins co-immunoprecipitated with β1-YFP and β2-YFP; co-IP of protein extracts from plants expressing GFP (*Pro35S:GFP*) was used as negative control. B, GO terms of biological processes enriched in the β1-YFP and β2-YFP co-IPs. C, Diagrams of AP-1 and AP-2 complexes with their constituting subunits. Arabidopsis β1 and β2 are shared by AP-1 and AP-2. D, BiFC assay in *N. benthamiana* leaves showing positive interactions of β1 and β2 with the other three subunits of AP-1 and AP-2. YN or YC alone were used as negative controls. E, Quantification of percentage of cells with YFP signal in BiFC assay (15 randomly chosen regions of interest of infiltrated leaves from three biological replicates were analyzed). A *t* test was used to compare binding partners with their corresponding negative control; *, **, and *** indicate $P < 0.05$, $P < 0.01$, and $P < 0.001$, respectively; ns, nonsignificant. Graph represents means and error bars indicate SD. Scale bars = 50 μm.

GUS-stained anthers at developmental Stages 7–12 as defined by Sanders et al. (1999). We found that while *β2* was weakly expressed in developing anthers, *β1* expression was strong in the tapetum and microspores from Stage 9 up to completion of pollen development (Stage 12) (Figure 2C), suggesting that β1 may have a predominant role in pollen development.

To analyze the subcellular localization of β1 and β2, we imaged *Proβ1:β1-YFP* and *Proβ2:β2-YFP* plants by confocal microscopy. In meristematic root cells and developing pollen grains, both β1-YFP and β2-YFP localized to cytoplasmic foci and to the plasma membrane; however, in tapetal cells, both adaptins were almost exclusively detected in cytoplasmic foci (Figure 3, A–D).

Next, to determine the nature of the cytoplasmic foci, we co-expressed β1-YFP and β2-YFP with several subcellular markers, including VHAa1-RFP and VTI12-mCherry for TGN, CLC2-mKO for clathrin, and SYP22-RFP for vacuole. Both

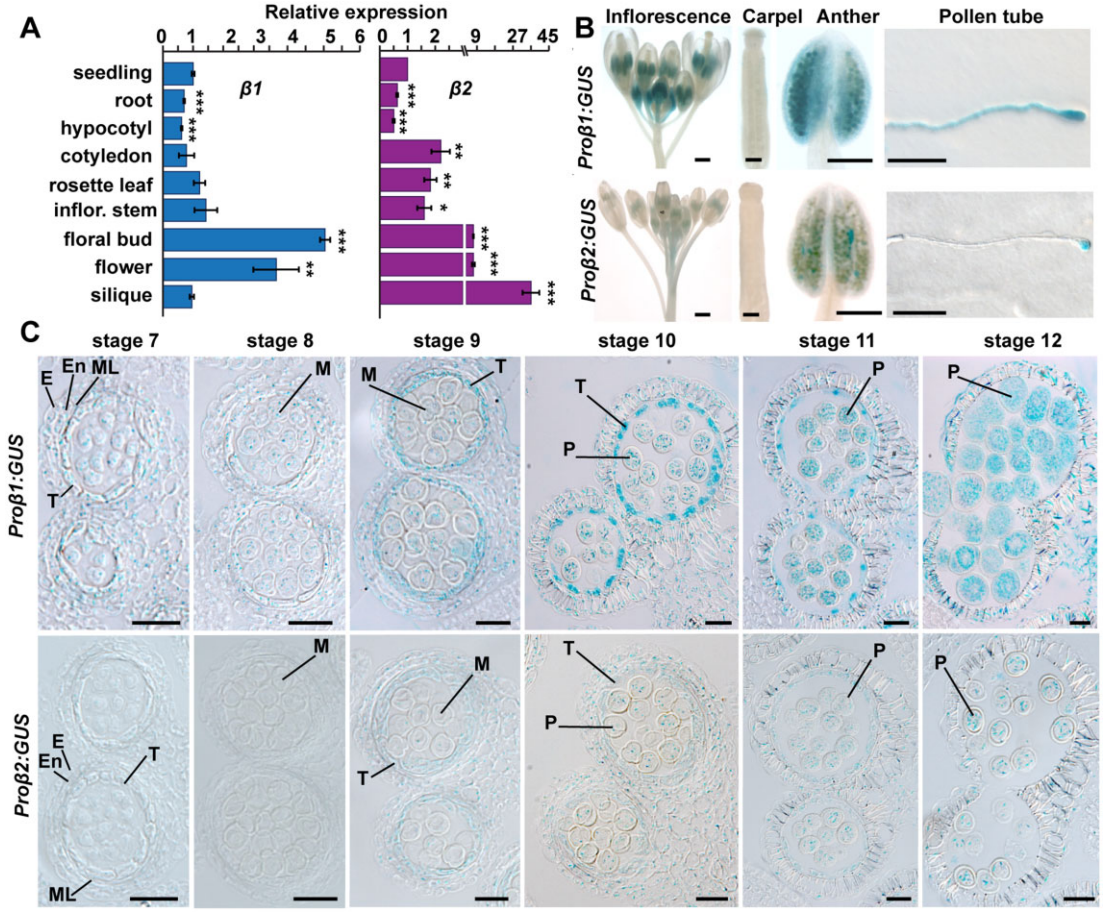

Figure 2 Expression of *β1* and *β2* in vegetative and reproductive organs. A, RT-qPCR analysis of *β1* and *β2* transcripts. Expression of each *β* adaptin gene was normalized to *ACTIN2* transcript levels and compared to the expression of 5-day-old whole seedlings as reference. Total RNA was isolated from the 5-day-old seedlings, roots, hypocotyls, cotyledons, rosette leaves, inflorescence stems, floral buds, flowers, and siliques of WT plants. The graphs show one representative assay of three replicates. Bars represent means and error bars indicate SD. A *t* test was used to compare expression in different tissues to the 5-day-old seedling; *, **, and *** indicate $P < 0.05$, $P < 0.01$, and $P < 0.001$, respectively. B, GUS staining of inflorescences, carpels, anthers, and pollen tubes germinated in vitro for 3 h from *Proβ1:GUS* and *Proβ2:GUS* transgenic plants. C, Sections of developing anthers from *Proβ1:GUS* and *Proβ2:GUS* transgenic plants. The GUS signal in tapetum and pollen grains in *Proβ1:GUS* is stronger than in *Proβ2:GUS* plants throughout anther development. E, epidermis; En, endothecium; ML, middle layer; T, tapetum; M, microspore; P, pollen grain. Scale bars = 1 mm in (B) (inflorescence), 200 μm in (B) (carpel and anther), 25 μm in (B) (pollen tube), and 20 μm in (C).

β1-YFP and β2-YFP showed high colocalization (Pearson's correlation coefficients = 0.71–0.94) with VHAa1-RFP, VTI12-mCherry, and CLC2-mKO on the cytoplasmic foci of tapetal cells and pollen grains (Figure 3, E and F; Supplemental Figure S4), indicating that these organelles are TGNs.

β1 and β2 adaptins are required for endocytosis and exocytosis in root cells

To characterize the function of the two β adaptins in Arabidopsis, we identified two mutants for *β1*, *β1-1* and *β1-2*, and one for *β2*, *β2-1* (Supplemental Figure S5A). Based on the lack of amplification of full-length *β1* or *β2* transcripts, we concluded that the three lines were transcript-null mutants, although, based on our RT-PCR results, *β1-1* produces a truncated transcript containing the region upstream of the T-DNA insertion (Supplemental Figure S5B). These three single mutant lines showed no detectable phenotypic defects during either vegetative or reproductive development (Supplemental Figures S5, C–E and S6, A–C). Therefore, we generated double mutants by crossing *β1-1* and *β1-2* with *β2-1* plants. Plants that were homozygous mutants for either β adaptin gene and heterozygous for the other one (*β1-1 β2-1/+*, *β1-1/+ β2-1*, *β1-2 β2-1/+*, and *β1-2/+ β2-1*) produced smaller rosettes and shorter inflorescence stems compared to WT and single mutants (Supplemental Figure S5, C–E), suggesting functional redundancy between the two genes. However, we were unable to obtain double homozygous mutant plants among the progeny of these four self-pollinated lines (Supplemental Table S5), suggesting that loss of function of both *β1* and *β2* leads to gametophytic or embryo lethality.

To better understand the function of β1 and β2 in vegetative tissues, we analyzed endocytic and exocytic trafficking in root cells of 5-day-old *β1-1 β2-1/+* seedlings. We incubated seedlings in 2-μM of the endocytic dye FM4–64 for 10 min and measured the amount internalized after a

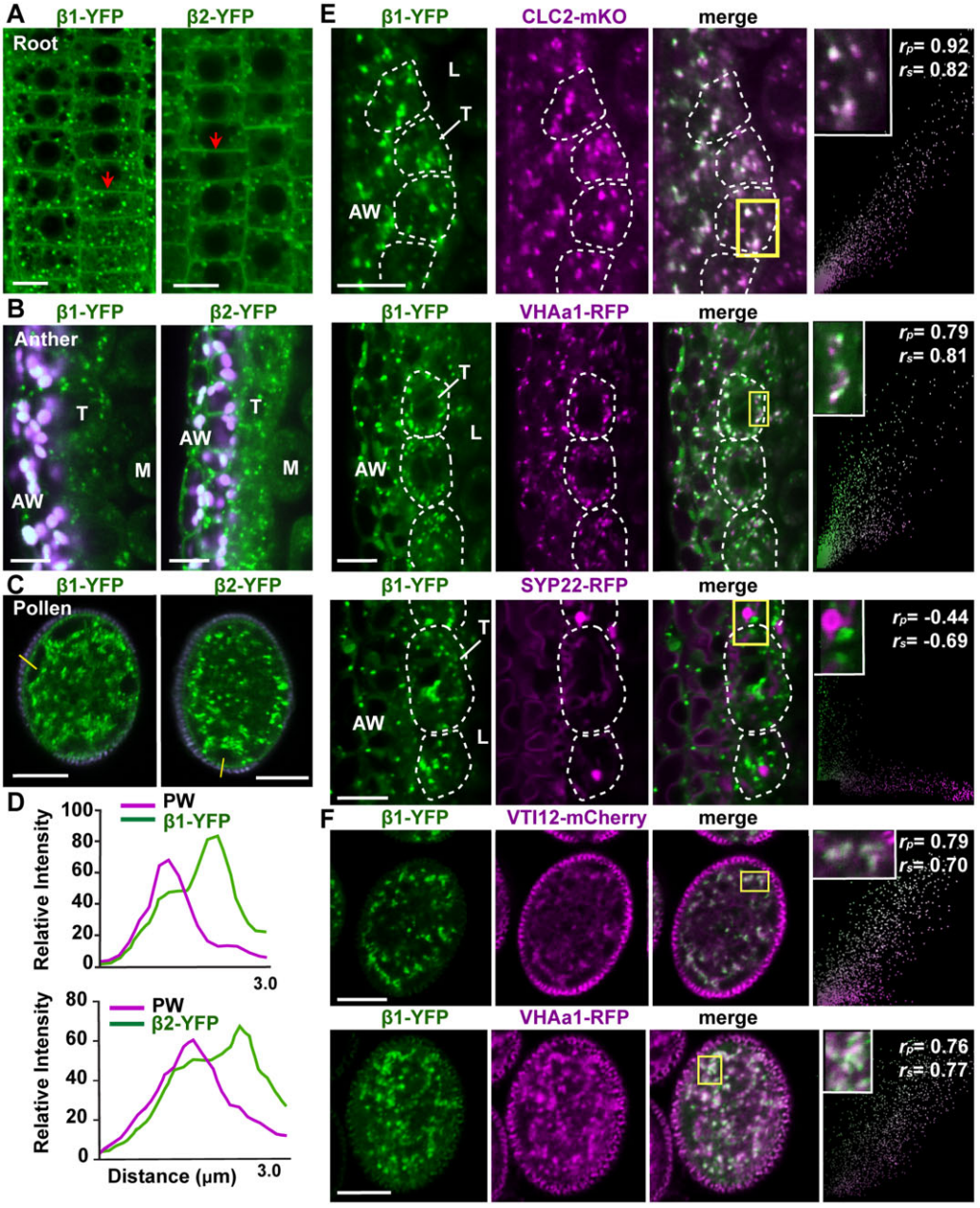

Figure 3 Subcellular localization of β1-YFP and β2-YFP. A–C, β1 and β2 are localized to the plasma membrane (PM) (arrows in A) and cytoplasmic puncta in meristematic root cells (A) and pollen grains (C), but almost exclusively to cytoplasmic foci in tapetal cells (B). Chlorophyll autofluorescence is shown in magenta. D, Fluorescence intensity profiles were calculated along the lines indicated in (C) to show spatial separation of pollen wall (PW) autofluorescence from the β1-YFP and β2-YFP signals at the PM. E, β1-YFP colocalizes with the TGN-localized CLC2-mKO and VHAa1-RFP but not with the vacuolar marker SYP22-RFP in tapetum. F, β1-YFP colocalizes with the TGN markers VTI12-mCherry and VHAa1-RFP in pollen grains. The last column to the right in (E) and (F) shows colocalization between fluorescence signals and the linear Pearson's correlation coefficient (PCC) (r_p) and the nonlinear Spearman's rank correlation coefficient (r_s) within the boxed areas indicated in the merged images; r = 1.0 means complete colocalization. Dashed lines define the boundaries of tapetal cells. AW, anther wall; T, tapetum; L, locule; M, microspore. Scale bars = 10 μm.

15 min chase by calculating the ratio between the intracellular and plasma membrane-localized FM4–64 signals. The *β1-1 β2-1/+* root cells internalized significantly less FM6–64 than the WT control (Figure 4, A and B). We then expressed the auxin efflux carrier PIN2 fused to GFP (*ProPIN2:PIN2-GFP*) in the *β1-1 β2-1/+* mutant seedlings and treated them with 50-μM of cycloheximide (CHX) for 30 min to block protein synthesis, followed by a 30 min treatment with CHX plus 50-μM brefeldin A (BFA), a drug that inhibits post-Golgi trafficking (Rosa et al., 1992) and leads to the aggregation of TGN clusters also called BFA bodies (Tse et al., 2006). Under these conditions, exocytosis of newly synthesized proteins is highly

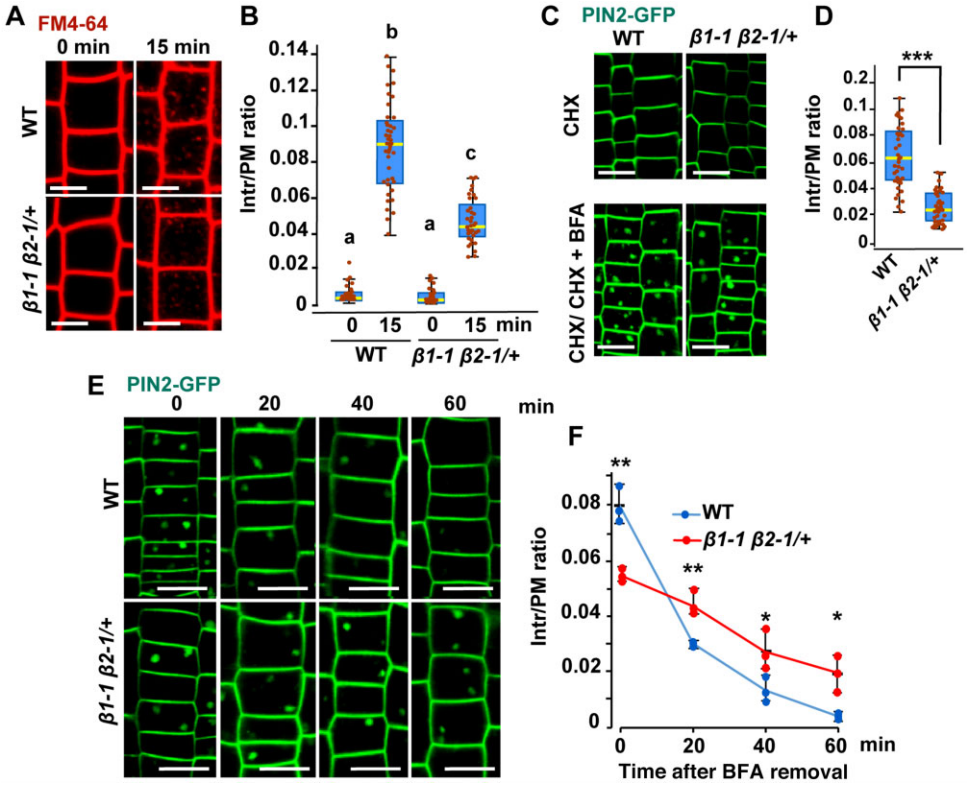

Figure 4 Trafficking defects in *β1 β2* double mutant roots. A, Root cortex cells stained with FM4–64. Five-day-old seedlings were incubated with 2-μM FM4–64 for 10 min; confocal imaging was performed right after incubation (time 0) and 15 min later. B, Quantification of FM4–64 signal intensity ratio between the PM and cell interior (Intr) (n = 40 cells from five roots were measured; the experiment was repeated 3 times with similar results). C, Imaging of PIN2-GFP in root cells treated with 50-μM CHX for 30 min followed by treatment with 50-μM BFA plus 50-μM CHX for 30 min. D, Quantification of PIN2-GFP signal intensity ratio between the PM and Intr after CHX/CHX + BFA treatment as described in (C) (n = 40 cells from five roots were measured; the experiment was repeated 3 times with similar results). In (B) and (D), box and whisker plots display the variation in data through quartiles; the middle line indicates the median and whiskers show the upper and lower fences. Different letters on graphs indicate significant difference ($P < 0.05$) calculated by one-way ANOVA followed by Tukey's test. *** indicate $P < 0.001$. E, PIN2-GFP re-localization in roots after washout of CHX and BFA. Seedlings were pretreated with 50-μM CHX for 30 min, followed by 50-μM BFA plus 50-μM CHX for 60 min, and final wash out with fresh 0.5 × MS liquid medium. Imaging was performed right after washout and at 20-min intervals after washout. F, Quantification of PIN2-GFP signal intensity ratio between the PM and Intr. The graph shows the average of three experiments and SD; for each experiment, at least 40 cells from 5 roots were measured. A t test was used to compare values between genotypes at each time point. * and ** indicate $P < 0.05$ and $P < 0.01$, respectively. Scale bars = 10 μm.

reduced due to the presence of CHX whereas endosomal recycling is impaired by BFA. Therefore, the resulting BFA bodies contained mostly the PIN2-GFP pool internalized from the plasma membrane via endocytosis. We detected a significant reduction in the PIN2-GFP signal at BFA bodies in the *β1-1 β2-1/+* mutant root cells compared to controls (Figure 4, C and D), consistent with impaired endocytosis (Figure 4, A and B). To assess exocytosis/endosomal recycling traffic to the plasma membrane, after a 60 min incubation with both CHX and BFA, we washed out both chemicals and chased the redistribution of PIN2-GFP by calculating the ratio intracellular to plasma membrane PIN2-GFP fluorescence signal over time (20, 40, and 60 min after CHX and BFA washout). We found that the re-localization of PIN2-GFP from the BFA bodies to the plasma membrane was significantly delayed in the *β1-1 β2-1/+* mutant root cells compared to WT (Figure 4, E and F). These results suggest that β1 and β2 are required for both efficient exocytosis and endocytosis, consistent with their participation in the AP-1 and AP-2 complexes, respectively.

β1 and β2 adaptins are important for plant fertility, pollen morphology, and pollen tube growth

As we failed to obtain a double homozygous mutant, we analyzed the function of β1 and β2 in plant fertility by measuring ovule/seed abortion in developing siliques of single and double mutants. Whereas WT and single mutant plants showed on average <3% ovule/seed abortion rates, between 22% and 55% of the ovules/seeds aborted in the siliques produced by the four double mutant lines (*β1-1 β2-1/+*, *β1-1/+ β2-1*, *β1-2 β2-1/+*, *β1-2/+ β2-1*) (Figure 5A).

Reciprocal crosses between WT and the four double mutants, as either male (pollen) or female (embryo sac) donors, indicated that there was no male and only partial female transmission of the *β1 β2* double mutations (Supplemental Table S5). This suggests that, although β1

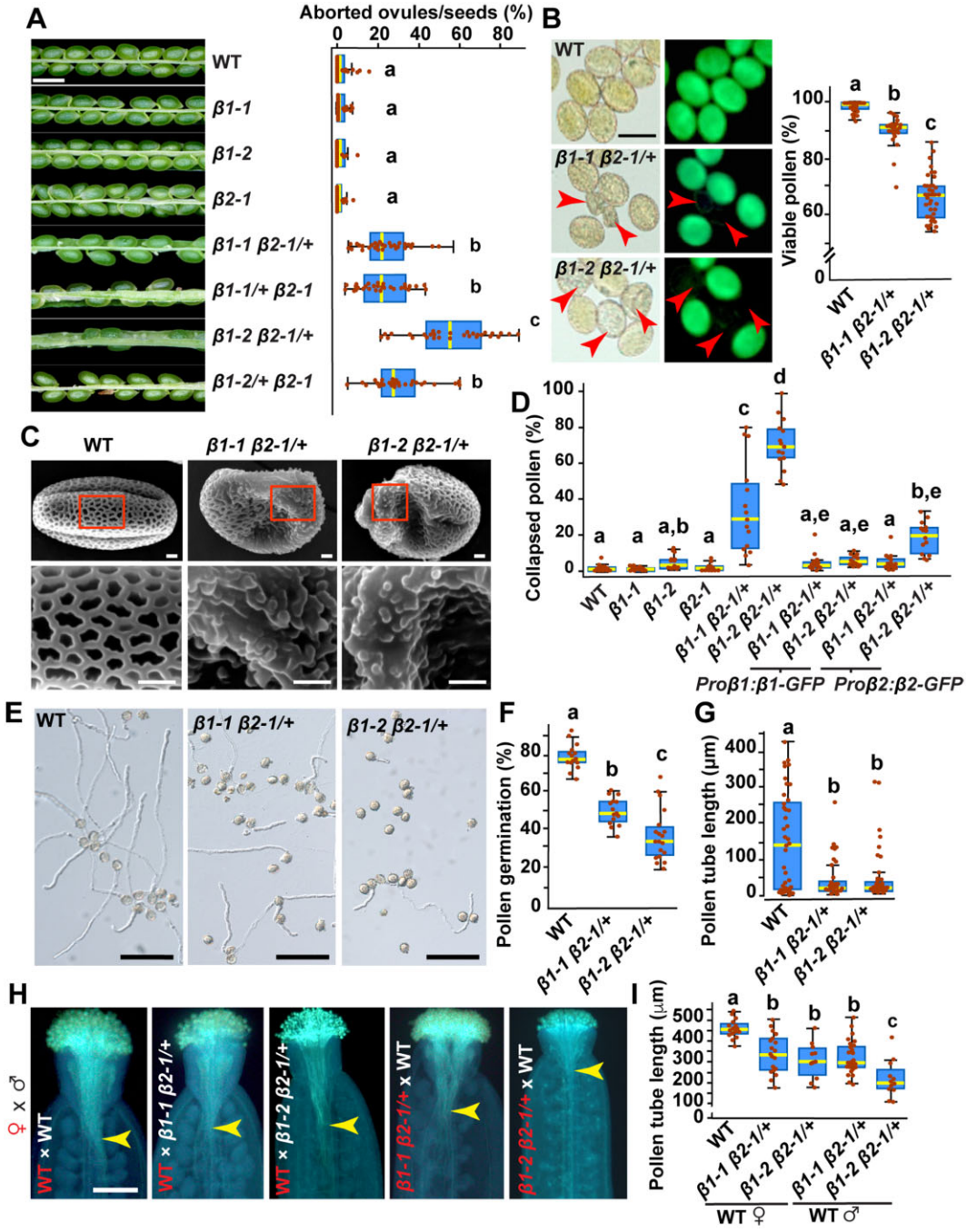

Figure 5 Male fertility defects in *β1 β2* double mutants. A, Dissected siliques and the corresponding quantification data showing aborted ovules/seeds in self-pollinated WT and *β1 β2* single and double mutant plants (30 siliques from three biological replicates were quantified for each genotype). B, Pollen viability quantification by FDA staining in WT and *β1 β2* double mutants. Pollen from dehiscing anthers was analyzed. Arrowheads show unstained, inviable pollen grains. C, Scanning electron micrographs of exine patterns from WT and *β1 β2* double mutants. Bottom images are the magnified areas marked by a box in the images above. D, Quantification of collapsed pollen grains (at least from 15 anthers in three biological replicates were analyzed for each genotype; each biological replicate consisted of at least 5 anthers). E, Pollen grains germinated after 3 h of *in vitro* culture. Pollen grains were isolated from WT and *β1 β2* double mutant anthers. F, Quantitative analysis of pollen germination rates at 3 h under *in vitro* conditions (pollen grains from at least 15 anthers in three biological replicates were analyzed for each genotype). G, Pollen tube length grown for 3h in *in vitro* culture from pollen grains of WT and *β1-1 β2-1/+* and *β1-2 β2-1/+* double mutant anthers (40 pollen tubes were measured for each genotype). H, Representative images of aniline blue staining of pollen tubes from reciprocal crosses between WT and *β1 β2* double mutants 4 h after hand-pollination. Arrowheads indicate the position of pollen tube tips. I, Pollen tube length after 4 h of hand-pollination (15, 19, 11, 27, 12 pistils were measured for WT♀× WT, WT♀× *β1-1 β2-1/+*, WT♀× *β1-2 β2-1/+*, *β1-1 β2-1/+*♀× WT, *β1-2 β2-1/+*♀× WT, respectively). Box and whisker plots display the variation in data through quartiles; the middle line indicates the median and whiskers show the upper and lower fences. Different letters on graphs indicate significant difference ($P < 0.05$) calculated by one-way ANOVA followed by Tukey's test. Scale bars = 1 mm in (A), 100 μm in (B), 20 μm in (C), 200 μm in (E) and (H).

and β2 are needed for both female and male gametophytic development, they are essential only for pollen function.

To understand what aspects of pollen function are controlled by β1 and β2, we first examined the viability of mature pollen grains by fluorescein diacetate (FDA) staining, which results in a strong fluorescence signal only in living pollen (Heslop-Harrison and Heslop-Harrison, 1970). We found that 89.6% (±2%; n = 1,095 pollen grains in 24 anthers) and 68.7% (±8%; n = 913 pollen grains in 38 anthers) of the pollen grains in *β1-1 β2-1/+* and *β1-2 β2-1/+* anthers, respectively, were alive, whereas 98.5% (±2%; n = 1,110 pollen grains in 22 anthers) of the WT pollens were viable (Figure 5B). Similar results were obtained using Alexander's pollen vitality stain (Alexander, 1969) (Supplemental Figure S7, A and B).

The mutant pollen grains that failed to stain with FDA were shrunken with collapsed walls (Figure 5B). Arabidopsis pollen grains develop three main cell wall layers: the innermost intine made of cellulose, pectin, and other polysaccharides; the exine containing sporopollenin; and the tryphine or pollen coat, containing waxes and filling the exine crevices (Blackmore et al., 2007; Ariizumi and Toriyama, 2011). Using scanning electron microscopy imaging, we observed that the shrunken pollen grains formed by double mutant plants tend to cluster together and showed sectors with abnormal exine morphology, consisting of irregular bacula instead of the typical reticulate pattern of the WT pollen grains (Figure 5C; Supplemental Figure S7C). We then quantified the proportion of morphologically abnormal pollen grains. In the WT and single *β1* and *β2* mutants, we found that 1%–4% of pollen grains were collapsed, whereas ∼40% and 70% of the pollen grains from *β1-1 β2-1/+* and *β1-2 β2-1/+* anthers, respectively, were shrunken or deformed (Figure 5D). Considering that in the mutants, we detected a lower proportion of inviable pollen using both the FDA and Alexander's stains (averages of 10%–23% and 32%–33% in *β1-1 β2-1/+* and *β1-2 β2-1/+*, respectively; Figure 5B; Supplemental Figure S7, A and B), we hypothesized that some of the shrunken mutant pollen grains while alive, and may not be fully capable of fertilizing embryo sacs.

Therefore, we analyzed pollen germination and pollen tube growth using both *in vitro* and *in vivo* (pollen tube growth in intact carpels) assays (Figure 5, E–I). After 3 h *in vitro* culture, over 70% of the WT pollen had germinated, whereas < 50% and 25% of the pollen grains from *β1-1 β2-1/+* and *β1-2 β2-1/+* plants, respectively, had formed pollen tubes (Figure 5, E and F). In addition, the mutant pollen grains that did germinate, produced pollen tubes significantly shorter compared to those of WT pollen grains (Figure 5G). When allowed to germinate on the surface of WT stigmas, pollen grains from both *β1-1 β2-1/+* and *β1-2 β2-1/+* plants showed a statistically significant decrease in pollen tube length compared to WT pollen (Figure 5, H and I), further confirming the notion that, although viable, pollen grains from double mutant plants show defective pollen tube growth. Interestingly, in similar assays, when WT pollen grains were applied to stigmas of either *β1-1 β2-1/+* or *β1-2 β2-1/+* plants, we also observed a significant decrease in pollen tube growth compared to controls (Figure 5, H and I). Taken together, these results indicate that mutant pollen grains are compromised in both germination and pollen tube growth and that the mutant carpel is less proficient in supporting pollen tube growth compared to the WT.

The expression of either *Proβ1:β1-GFP* or *Proβ2:β2-GFP* in the *β1-1 β2-1/+* and *β1-2 β2-1/+* mutant lines largely restored normal pollen grain morphology and viability and seed development (Figure 5D; Supplemental Figure S6, D and E; S7, A–C), indicating that GFP-tagging of β adaptins does not affect their function and that the fertility defects seen in the double mutant lines are indeed linked to mutations in the β1 and β2 adaptins.

β1 and β2 adaptins are required for exine formation

To investigate defects in pollen formation in the double mutant lines, we performed a histological analysis of anthers at different developmental stages. In WT, *β1-1 β2-1/+*, and *β1-2 β2-1/+* anthers, morphologically normal tetrads formed at the end of meiosis (Stage 7) and developed into free microspores with noticeable pollen walls by Stage 9 (Figure 6A). However, at Stage 10, some microspores of *β1-1 β2-1/+* and *β1-2 β2-1/+* plants showed abnormally enlarged vacuoles compared to those in WT (Figure 6A, arrowheads). By Stage 11, some microspores in mutant anthers had aborted, while others seemed to develop normally (Figure 6A). In terms of the anther wall (sporophytic tissue), all layers, including epidermis, endothecium, middle layer, and tapetum seemed to differentiate normally in the *β1-1 β2-1/+* and *β1-2 β2-1/+* mutant plants (Figure 6A).

To better understand the structural defects associated with abnormal pollen development in mutant anthers, we performed imaging by transmission electron microscopy of anthers at Stage 10 when microspore abortion becomes noticeable. Whereas at this developmental stage, WT microspores have developed well-defined bacula and tectum as part of their exine, the abnormally vacuolated microspores in the mutant anthers showed shorter and wider bacula and no noticeable tectum (Figure 6B). Together, our results show that β1 and β2 adaptins are required for proper exine assembly and normal progression of microspore development.

β1 and β2 adaptins play a critical role in the trafficking of ATP-binding cassette G9 (ABCG9) and ABCG16 in tapetal cells

The microspore defects seen in the double mutant plants could be due to functions of β1 and β2 in gametophytic (i.e. microspores) and/or sporophytic tissues (i.e. anther wall layers). Because exine formation depends on the activity of the sporophytic tapetal cells, which secrete sporopollenin precursors into the locule through the action of plasma membrane transporters, we hypothesized that β1 and β2 adaptins regulate pollen wall development through their vesicle trafficking function in the tapetum. To test this

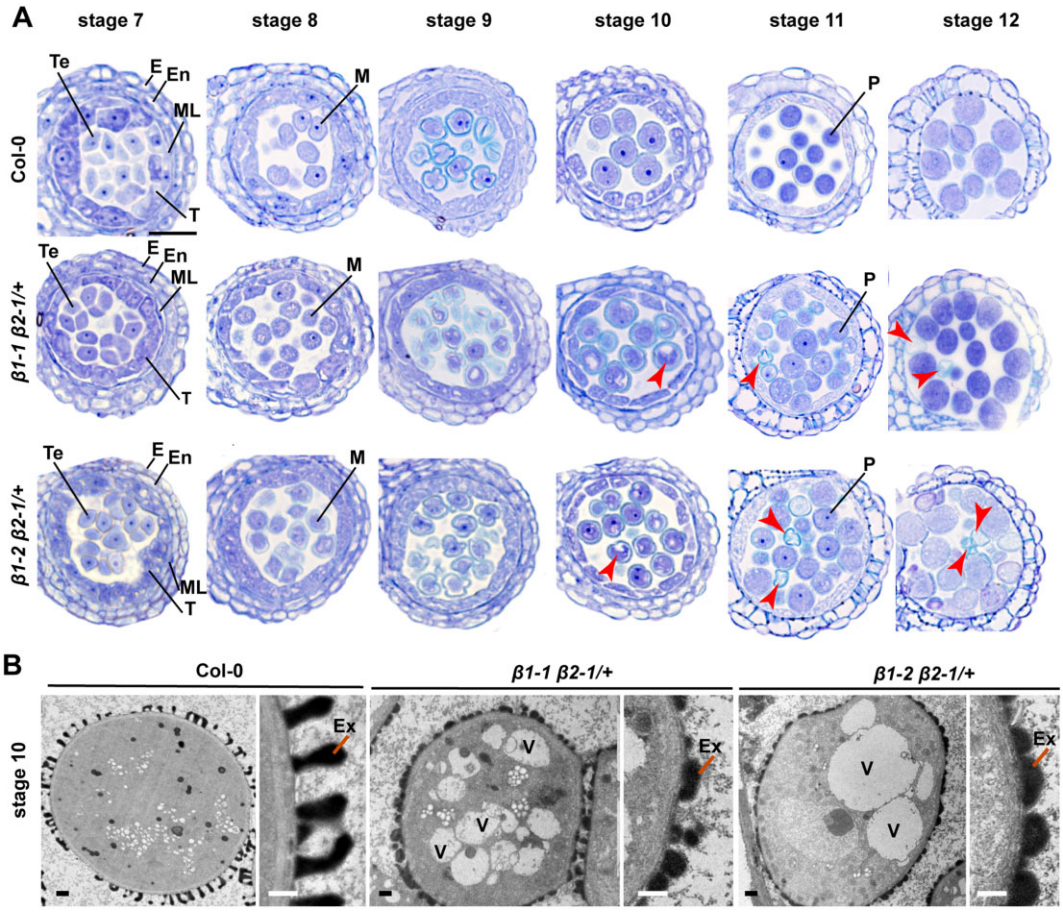

Figure 6 Abnormal pollen development in the *β1 β2* double mutants. A, Toluidine blue-stained cross-sections of developing anthers from WT and *β1-1 β2-1/+* and *β1-2 β2-1/+* double mutants. Tetrad development at Stage 7 and release of free microspores at Stages 8 and 9 seemed normal in mutant anthers. At Stage 10, some abnormally vacuolated microspores became evident in mutant anthers. At Stages 11 and 12, degenerated pollen grains (arrowheads) were visible in mutant but not in WT anthers. Te, tetrads. B, Transmission electron micrographs of pollen grains at Stage 10. Compared to WT, pollen grains from *β1-1 β2-1/+* and *β1-2 β2-1/+* mutant plants exhibit enlarged vacuoles and abnormal exine. V, vacuole; Ex, exine. Scale bars = 20 μm in (A), 1 μm in (B).

hypothesis, we expressed β1-YFP in *β1-1 β2-1/+* mutant plants under the control of promoters that are active specifically in either the tapetum (*ProA9*) (Paul et al., 1992) or microsporocytes and microspores (*ProARF17*) (Yang et al., 2013) (Figure 7, A and B). We found that the expression of β1-YFP in the tapetum but not in microsporocytes and microspores was able to fully restore normal pollen morphology and pollen viability compared to WT (Figure 7, A–C). To determine whether the tapetum-specific expression of β1/2 adaptins was also able to restore normal pollen function, we analyze pollen germination rates *in vitro*. We found that the morphologically normal pollen grains from *β1-1 β2-1/+* mutant anthers expressing *ProA9: β1-YFP* showed drastically reduced germination rate, similar to those of pollen from the *β1-1 β2-1/+* mutant and the *β1-1 β2-1/+* mutant expressing *ProARF17: β1-YFP* (Figure 7, D and E). Taken together, our results suggest that the expression of β1/2 adaptins in tapetal cells is important for normal pollen formation but not enough to restore normal pollen performance during germination in *β1 β2* mutants.

Next, we analyzed the potential roles of β1/2 adaptins in tapetal cells during the formation of pollen grains. The export of pollen wall precursors from the tapetal cells into the anther locule is a rather complex process that depends on several trafficking pathways and plasma membrane transporters, including ATP-binding cassette (ABC)G9 and ABCG16 (Choi et al., 2014; Yim et al., 2016; Goodman et al., 2021). Since the AP-2 complex has been shown to participate in clathrin-mediated endocytosis and recycling of another ABCG transporter, ABCG25, in Arabidopsis seedlings (Park et al., 2016), we hypothesized that β1 and β2 may be required for proper localization and/or trafficking of ABCG9 and ABCG16 in tapetal cells. Therefore, we expressed ABCG9-YFP and ABCG16-YFP in mutant and WT lines and analyzed their subcellular localization in tapetal cells of developing anthers by confocal microscopy (Figure 8, A–D). In WT and the single *β1-1* and *β2-1* mutant anthers between Stages 6 and 8, ABCG9-YFP and ABCG16-YFP were detected at the plasma membrane, as previously reported (Choi et al., 2014; Yim et al., 2016; Goodman et al., 2021). However, in

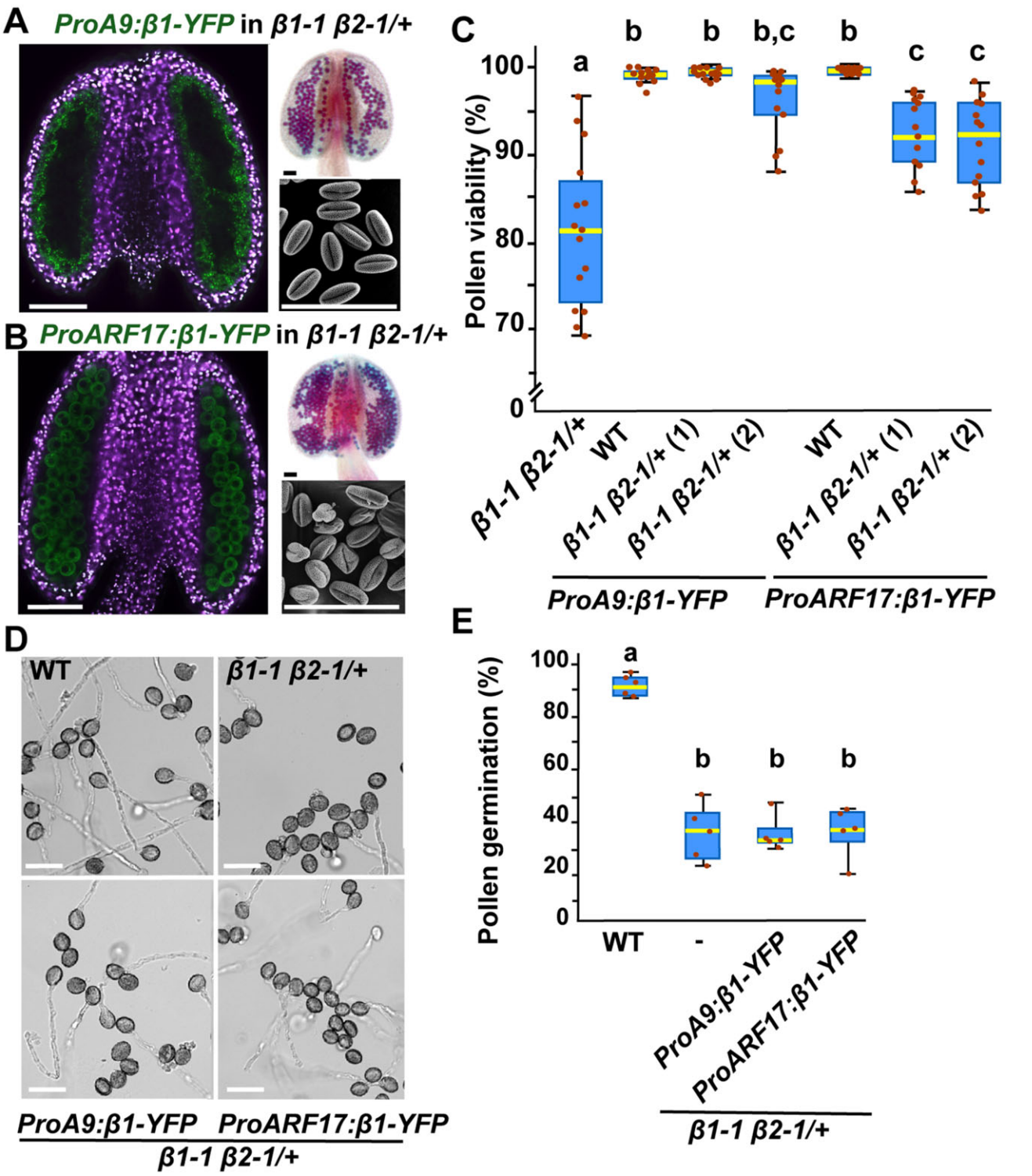

Figure 7 Effects of tissue-specific expression of β1-YFP in the *β1 β2* double mutant. A and B, Tissue-specific expression of β1-YFP seen by confocal imaging, Alexander's viability test, and scanning electron micrographs of pollen grains from *β1-1 β2-1/+* mutant plants expressing either *ProA9:β1-YFP* in tapetum (A) or *ProARF17:β1-YFP* in microspores (B). Chlorophyll autofluorescence is shown in magenta. C, Quantification of pollen viability in *β1-1 β2-1/+* anthers expressing *ProA9:β1-YFP* or *ProARF17:β1-YFP*. (1) and (2) indicate two independent transgenic lines. At least 3,000 pollen grains from 15 anthers in three replicates were analyzed for each genotype. D, Pollen grains germinated after 3 h of *in vitro* culture. Pollen grains were isolated from WT, *β1 β2* double mutant, and *β1 β2* double mutant lines expressing either *ProA9:β1-YFP* or *ProARF17:β1-YFP*. E, Quantitative analysis of pollen germination rates at 3 h under *in vitro* conditions (graph shows one representative assay with five flowers of each genotype; the experiment was repeated 3 times with similar results). For all graphs, box and whisker plots display the variation in data through quartiles; the middle line indicates the median and whiskers show the upper and lower fences. Different letters on graphs indicate significant difference ($P < 0.05$) calculated by one-way ANOVA followed by Tukey's test. Scale bars = 50 μm.

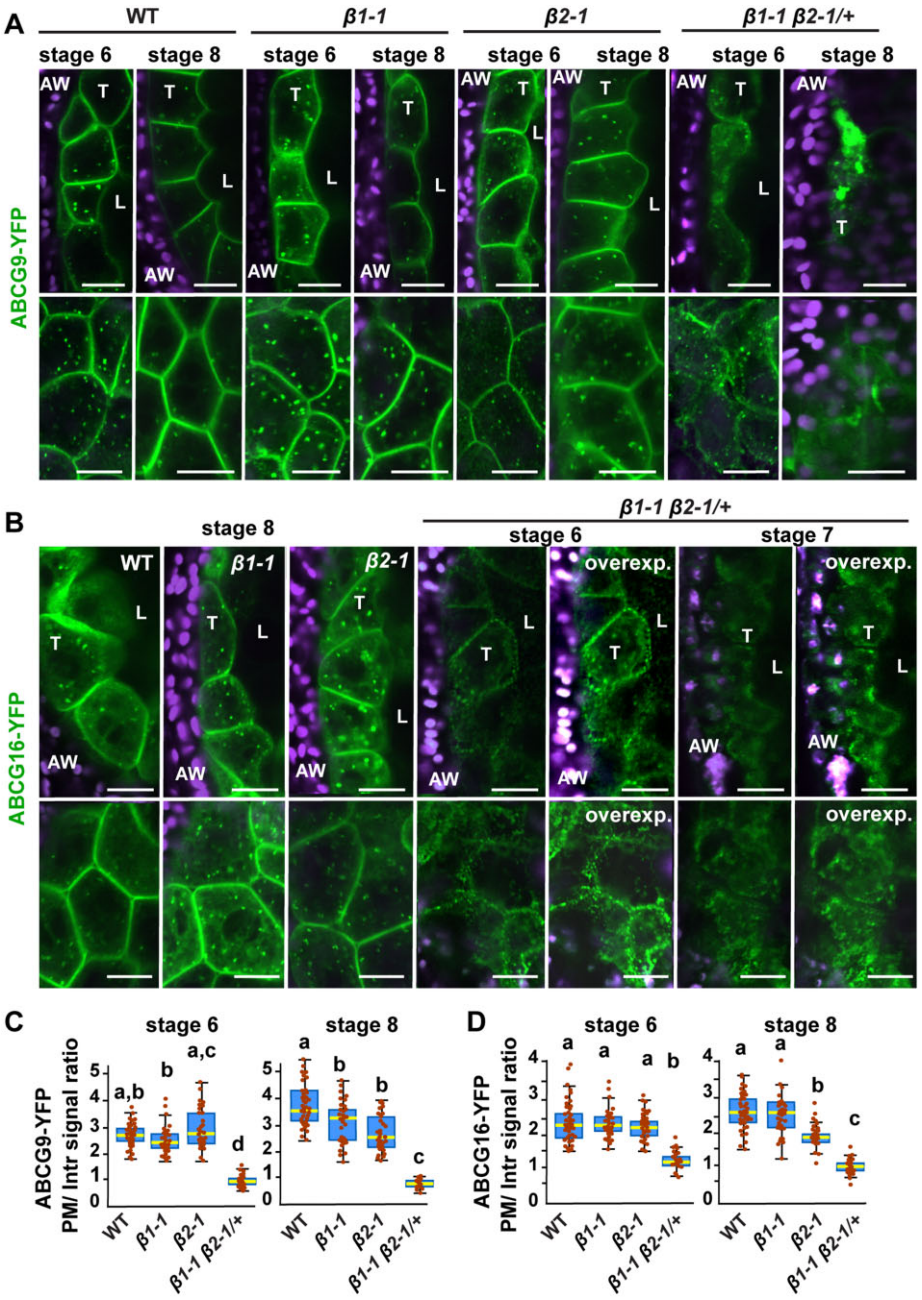

Figure 8 Abnormal localization of ABCG9-YFP and ABCG16-YFP in *β1 β2* double mutant tapetal cells. A and B, Localization of ABCG9-YFP (A) and ABCG16-YFP (B) in anthers (Stages 6 and 8) seen in confocal images collected through the middle of the locule (upper row) or from the surface of the tapetal layer (tangential view; lower row) in WT and *β1* and *β2* single and *β1-1 β2-1/+* double mutants. Over-exposed images (overexp.) in (B) are included to better visualize the weak signal of ABCG16-YFP in tapetal cells. C, Quantification of the ratio of the ABCG9-YFP signal intensity between the PM and cell interior (Intr) (n = 42 cells from 7 WT anthers, 30 cells from 5 *β1-1* anthers; 30 cells from 5 *β2-1* anthers and 30 cells from 7 *β1-1 β2-1/+* anthers at Stage 6; n = 42 cells from 7 WT anthers, 35 cells from 6 *β1-1* anthers; 30 cells from 6 *β2-1* anthers,15 cells from 8 *β1-1 β2-1/+* anthers at Stage 8). D, Quantification of the ratio of the ABCG16-YFP signal intensity between the PM and Intr (n = 45 cells from 9 WT anthers, 30 cells from 4 *β1-1* anthers; 45 cells from 8 *β2-1* anthers and 34 cells from 10 *β1-1 β2-1/+* anthers at Stage 6. n = 42 cells from 6 WT anthers, 45 cells from 6 *β1-1* anthers; 45 cells from 8 *β2-1* anthers, 28 cells from 12 *β1-1 β2-1/+* anthers at Stage 8). Box and whisker plots display the variation in data through quartiles; the middle line indicates the median and whiskers show the upper and lower fences. Different letters on graphs indicate significant difference ($P < 0.05$) calculated by one-way ANOVA followed by Tukey's test. Scale bars = 10 μm.

the *β1-1 β2-1/+* double mutant, there was an overall decrease in the plasma membrane signal and an increased accumulation in intracellular puncta (Figure 8, A–D).

We reasoned that, since β1 and β2 localize almost exclusively to the TGN in tapetal cells (Figure 3, B and E; Supplemental Figure S4A), the cytoplasmic signal of ABCG9-YFP and ABCG16-YFP in the double mutant tapetum could

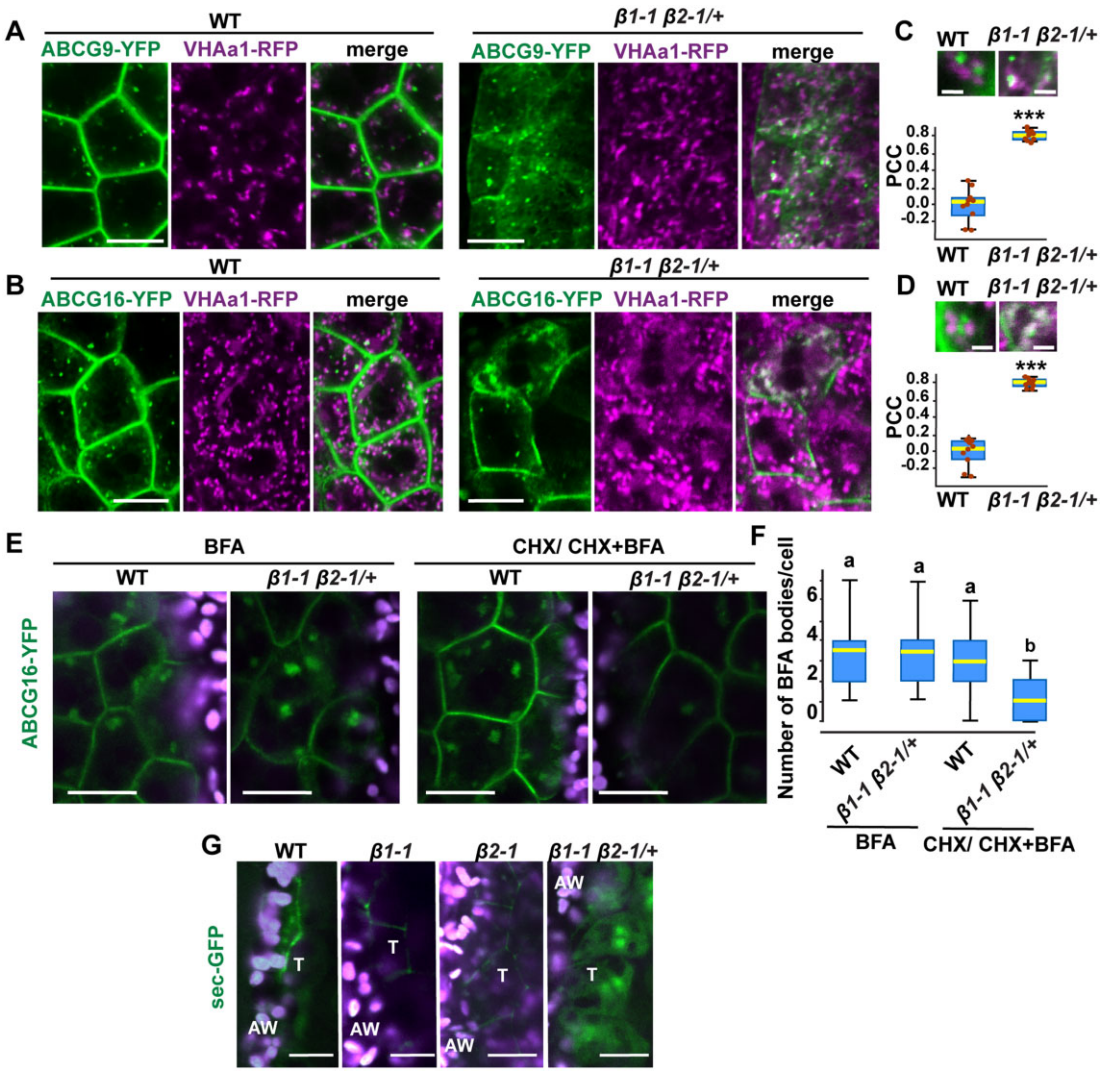

Figure 9 Defective post-Golgi trafficking in the *β1 β2* double mutant tapetal cells. A and B, Co-expression of ABCG9-YFP (A) and ABCG16-YFP (B) with VHAa1-RFP in control (WT) and *β1-1 β2-1/+* tapetal cells from anthers at Stage 7 and 8. C and D, Colocalization analysis between VHAa1-RFP and either ABCG9-YFP (C) or ABCG16-YFP (D). PCC for YFP and RFP signals were calculated in 10 randomly selected regions like the ones showed in (C) and (D). Asterisks indicate significant differences calculated by a *t* test ($P < 0.001$). E, Localization of ABCG16-YFP in the presence of BFA and BFA plus CHX in WT and *β1-1 β2-1/+* tapetal cells in anthers at Stages 7 and 8. F, Quantification of ABCG16-YFP-labeled BFA bodies per tapetal cell after BFA and BFA plus CHX treatments in WT and *β1-1 β2-1/+* anthers. For BFA treatment, 105 cells from 9 WT anthers and 105 cells from 10 *β1-1 β2-1/+* anthers were analyzed. For BFA plus CHX treatment, 75 cells from 8 WT anthers and 90 cells from 8 *β1-1 β2-1/+* anthers were analyzed. Error bars represent means ± SD. For all graphs, box and whisker plots display the variation in data through quartiles; the middle line indicates the median and whiskers show the upper and lower fences. Different letters in (F) indicate significant difference ($P < 0.05$) calculated by one-way ANOVA followed by Tukey's test. (G) Distribution of sec-GFP in WT and *β1-1 β2-1/+* tapetal cells at Stage 7. Scale bars = 10 μm.

result from defects in TGN trafficking. Therefore, we co-expressed both tagged ABCG transporters with the TGN marker VHAa1-RFP and found that, whereas there was almost no signal of the ABCG transporters at the TGN of WT tapetal cells, the cytoplasmic puncta enriched in ABCG9-YFP and ABCG16-YFP in the double mutant largely coincides with the TGN marker (Figure 9, A–D).

Although β1 and β2 adaptins are able to assemble into either the AP-1 complex involved in exocytosis from the TGN or the AP-2 complex involved in endocytosis from the plasma membrane (Figure 1, D and E; Supplemental Tables S1 and S2), in at least tapetal cells, their localization at the TGN suggests a predominant role in TGN-dependent trafficking. To further explore this possibility, we performed pharmacological treatments in WT and *β1-1 β2-1/+* double mutant anthers expressing ABCG16-YFP. We first treated anthers with 100-μM BFA. After 2 h in BFA, control and mutant tapetal cells show similar number of ABCG16-YFP-positive BFA bodies (Figure 9, E and F), although, as noticed before (Figure 8B), the ABCG16-YFP plasma membrane signal was diminished in the mutant tapetal cells. The ABCG16-YFP fluorescence signal from the BFA bodies could

derive from transporter molecules on their way to the plasma membrane (exocytic cargo) and/or recently internalized from the plasma membrane by endocytosis (endocytic cargo). To test these two possible scenarios, we pretreated anthers for 30 min with 100-μM CHX to block protein synthesis before incubation with both BFA and CHX for 2 h. Under these conditions, the synthesis of new ABCG16-YFP molecules is blocked and most of the fluorescent signal in BFA bodies should come from endocytosed molecules. In control anthers, we did not notice any reduction in the number of BFA bodies with CHX pretreatment (Figure 9, E and F). However, in the *β1-1 β2-1/+* double mutant tapetal cells, there was a sharp decrease in the number of ABCG16-YFP-positive BFA bodies (Figure 9, E and F), suggesting a limited endocytic contribution to BFA bodies. Taken together, these results suggest that in the *β1-1 β2-1/+* mutant tapetum, only a fraction of the newly synthesized ABCG9/16-YFP molecules reached the plasma membrane, whereas the rest are trapped at the TGN; as protein synthesis is inhibited in the presence of CHX, the ABCG16-YFP signal from BFA bodies in CHX + BFA-treated anthers fades more quickly in mutant than in control tapetal cells.

The overall weak signal of ABCG9/16-YFP at the plasma membrane and its accumulation in the TGNs of the *β1-1 β2-1/+* mutant tapetum together with the pharmacological treatments suggest that, although β1 and β2 adaptins are components of both AP-1 and AP-2 complexes in plants, their main role, at least in tapetal cells, is connected to AP-1-mediated post-TGN trafficking/secretion. To further verify this hypothesis, we introduced into the single and double mutant plants the sec-GFP reporter that contains a signal peptide and is secreted outside cells, where its fluorescence is quenched due to the acidic apoplastic pH (Zheng et al., 2004). In WT and single mutant anthers, sec-GFP was normally exported from the tapetal cells into the locule. However, in the *β1-1 β2-1/+* mutant, the same reporter accumulated inside tapetal cells (Figure 9G), confirming that β1 and β2 adaptins are required for exocytosis in tapetal cells.

To test whether β1 and β2 adaptins associate with ABCG9 and ABCG16, we tested their ability to interact with each other in both a yeast two-hybrid (Y2H) assay using a mating-based split ubiquitin system (mbSUS) and in a BiFC system. We found that in both assays, β1 and β2 associate with ABCG9 and ABCG16 (Figure 10, A–C), further supporting the notion that these adaptins are required for the proper trafficking of both ABCG transporters and suggesting that β adaptins mediate the binding of these cargo proteins to AP-1.

Discussion

We have identified β1 and β2 as two shared, large adaptins of the AP-1 and AP-2 complexes in Arabidopsis. The two β adaptins are, at least partially, functionally redundant and essential for male gametophytic development. We also uncovered a critical role of β1 and β2 in exocytic trafficking in tapetal cells during the late stages of pollen formation as they interact with and regulate the plasma membrane localization of the transporters ABCG9 and ABCG16, which are required for pollen wall assembly (Figure 11).

The β1 and β2 adaptins are shared by AP-1 and AP-2 in Arabidopsis

Within AP-1 and AP-2, β adaptins participate in the recruitment of clathrin and clathrin-accessory proteins. Clathrin itself does not interact with membranes and cargo proteins, and, therefore, its regulated recruitment to donor compartments is critical for vesicle trafficking. Although how exactly β adaptins engage clathrin heavy and light chains to form a clathrin coat has been a matter of recent debate (Chen and Schmid, 2020; Kovtun et al., 2020; Paraan et al., 2020; Smith et al., 2021), it is clear that the process is mediated by multiple binding sites in the hinge and ear domains of β adaptins and is essential for clathrin coat assembly. Some organisms, including nonmammalian animals, have only one β adaptin for both AP-1 and AP-2. Mammalian cells use specific β subunits for the AP-1 and AP-2 complexes; however, they have been shown to act at least partially redundantly. For example, elimination of the AP2β subunits causes only a mild reduction in the endocytic internalization of the transferrin receptor, due to the substitution of AP2β with AP1β (Keyel et al., 2008). Only fungi seems to have noninterchangeable β subunits for AP-1 and AP-2 (Dacks et al., 2008); however, the fungal β subunits of both AP-1 and AP-2 lack the canonical clathrin-binding domains and AP-2 has a clathrin-independent role in endocytosis in filamentous fungi (Martzoukou et al., 2017), suggesting that the fungal AP-1 and AP-2 complexes may have evolved divergent functions. We have found that the two putative AP1/2β subunits in Arabidopsis (β1 and β2) are able to co-assemble with subunits of both AP-1 and AP-2 (Figure 1), and consistently, localize to both TGN and plasma membrane (Figure 3, A and C), the cognate membranes for each complex.

Typically, AP-1 and AP-2 select cargo by binding two types of motifs in the cytoplasmic domains of plasma membrane proteins. The μ subunit binds tyrosine motifs (YxxΦ; where Y is a tyrosine, x is any amino acid, and Φ is a bulky, hydrophobic amino acid), whereas the α and σ subunit hemicomplex binds dileucine motifs (D/ExxxLL/I; where D is aspartate, E is glutamate, L is leucine, and I is isoleucine) (Doray et al., 2007). Very few examples are known where the β adaptins bind cargo proteins directly. For example, the mammalian β1 binds CD3γ, the subunit of the T-cell receptor, CD4, the T-cell co-receptor, Glut4, a glucose transporter, and mannose-6-phosphate receptor, through dileucine motifs at the TGN (Rapoport et al., 1998). Interestingly, the binding of β1 to dileucine motifs does not interfere with the binding of the μ subunit to tyrosine motifs in the same cargo proteins. In addition, both binding activities are differentially affected by phosphoinositides, indicating that the two sorting signals are recognized independently, and that their recognition is regulated separately (Rapoport et al., 1998). Our Y2H results suggest that

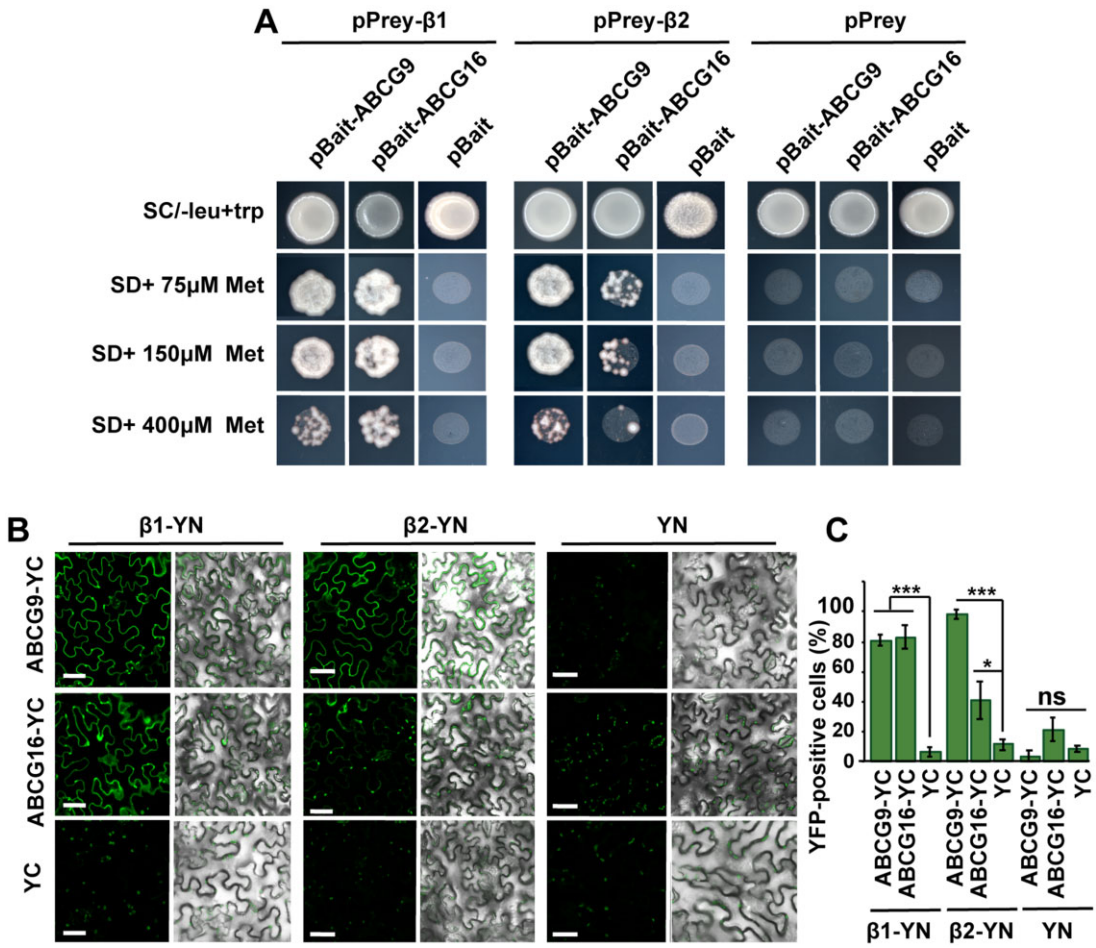

Figure 10 Interactions of β1 and β2 adaptins with ABCG9 and ABCG16 transporters. A, mbSUS Y2H assay showing positive interactions of β1 and β2 with ABCG9 and ABCG16. SC, synthetic complete medium; SD, synthetic minimal medium. Images are representative of three biological replicates. B, BiFC assay showing that β1 and β2 associate with ABCG9 and ABCG16 in epidermal cells of *N. benthamiana* leaves. For each tested pair, the left panels show YFP fluorescence whereas the right panels show the YFP fluorescence and brightfield merged images. C, Quantification of YFP-positive cells in BiFC assay (15 randomly selected regions of interest in infiltrated leaves from three biological replicates were considered for quantification). A *t* test was used to compare binding partners with their corresponding negative control; * and *** indicate $P < 0.05$, and $P < 0.001$, respectively. Graph represents mean ±SD. Scale bars = 50 μm.

Arabidopsis β1 and β2 can bind ABCG9 and ABCG16 (Figure 10), and consistently, both adaptins are required for the trafficking of the two transporters to the plasma membrane (Figure 8). Future studies will determine the motifs in ABCG9 and ABCG16 responsible for binding to β adaptins.

Mutants for individual adaptins of AP-1 or AP-2 consistently show growth defects and abnormal gametophytic development (Park et al., 2013; Teh et al., 2013; Wang et al., 2016, 2017; Feng et al., 2017; Shimada et al., 2018; Xu et al., 2022). Although the activities of AP-1 and AP-2 are interconnected, and therefore, disrupting the function of one of the AP complexes affects the dynamics of the other (Yan et al., 2021), loss of function of both β1 and β2 adaptins results in plant lethality and some common phenotypic defects with mutations in either AP-1 or AP-2 adaptins. For example, our pharmacological experiments showed that disruption of β1 and β2 adaptins caused impaired endocytosis and exocytosis in root cells (Figure 4), which is consistent with the disruption of both AP-1 and AP-2 complexes.

The unique features of tapetal cells as secretory cells

Plants with single mutations in either β1 or β2 are phenotypically normal but the plants with only one WT allele of either β adaptin produce a large proportion of abnormal pollen grains with defective walls, compromised viability, and reduced proficiency to generate pollen tubes (Figure 5). Morphological defects in developing microspores become evident at the anther developmental Stage 10 (Figure 6), when β1 is strongly expressed in tapetal cells (Figure 2C). Tapetal cells express plasma membrane transporters, including some of the ABCG subfamily, that mediate the secretion of pollen wall components into the anther locule (Quilichini et al., 2010, 2014; Choi et al., 2011, 2014; Dou et al., 2011; Kuromori et al., 2011). Thus, microspore development and the assembly of their complex walls depend on the membrane trafficking activity of both the microspore itself and the surrounding tapetal cells. When we tested in which cell type β1 was most critical for pollen development by driving

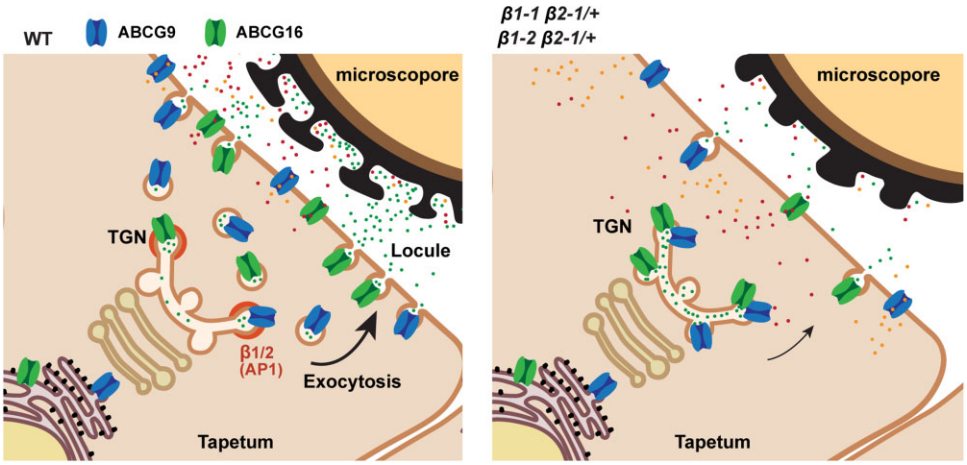

Figure 11 Model of β1/2 function in tapetal cells. In WT tapetal cells, β1 and β2 adaptins as part of the AP-1 complex (coats around the budding vesicle at the TGN) are required for post-TGN trafficking of ABCG9 and ABCG16 to the PM. Once at the PM of tapetal cells, ABCG9 and ABCG16 transport precursors for pollen wall assembly into the locule. In *β1 β2* double mutant tapetal cells, the newly synthesized ABCG9 and ABCG16 molecules failed to be efficiently transported to the PM and are instead retained at the TGN, resulting in abnormal pollen wall assembly and pollen abortion. Thick arrow indicates the normal exocytosis. Thin arrow indicates impaired exocytosis.

its expression with specific promoters (Figure 7), we found that although expression of β1 in microspores partially alleviates the pollen viability defects, its expression in tapetal cells fully restores pollen morphology and viability. This is consistent with the finding that two plasma membrane transporters, ABCG9 and ABCG16, expressed in tapetal cells and required for proper microspore development and pollen wall assembly, are mis-localized in the *β1-1 β2-1/+* mutant anther (Figure 8). However, pollen grains from *β1-1 β2-1/+* anthers expressing β1-YFP in tapetal cells showed impaired germination (Figure 7, D and E), suggesting that male gametophytic expression of β1/2 adaptins is also required for normal pollen germination and pollen tube growth.

Consistent with their shared role in assembly of AP-1, which acts in post-TGN trafficking, and AP-2, which participates in clathrin-mediated endocytosis, Arabidopsis β1 and β2 adaptins, localize to both the TGN and plasma membrane in root cells and developing pollen. However, at the tapetal cells, both adaptins localize almost exclusively to the TGN, raising the question of whether they play any relevant role in endocytosis at the plasma membrane. Consistent with this observation, the mis-localization of ABCG9 and ABCG16 from the plasma membrane to the TGN in *β1-1 β2-1/+* tapetal cells (Figure 8) and the quick loss of ABCG16-YFP signal from BFA bodies when mutant anthers were also treated with the protein synthesis-inhibitor CHX (Figure 9E), further supports a preferential role of β1 and β2 in anterograde, post-TGN trafficking in tapetal cells.

Why would β adaptins have a more important role in exocytosis (AP-1 function) than in endocytosis (AP-2 function) in the tapetum? Tapetal cells are emerging as a model for highly secretory plant cells with their own regulatory mechanisms. In Arabidopsis, the tapetum remains functional for only 4 days and then undergoes programmed cell death at late stages of pollen development. During its short life, the tapetum actively secretes enzymes and metabolites, which are essential for microspore development and pollen wall assembly (Smyth et al., 1990; Sanders et al., 1999). This highly coordinated exocytic activity seems to require a differential regulation of trafficking pathways. For example, tapetal cells seem to be hypersensitive to mutations in trafficking factors, including coat protein complex II (COPII) subunits required for vesicle-mediated trafficking between the endoplasmic reticulum (ER) and Golgi. Mutations in COPII components, such as SEC31, SEC23, and SAR1, have dramatic effects in tapetal cell function and pollen wall assembly (Fan et al., 2014; Zhao et al., 2016; Aboulela et al., 2018; Liang et al., 2020). The high demand for supporting exocytic activity in the tapetum is also evidenced by the strong tapetal expression of ECHIDNA, a TGN-localized protein that controls the secretion of a subset of plasma membrane proteins and is required for pollen formation (Fan et al., 2014). In addition, the ENDOSOMAL SORTING COMPLEX REQUIRED FOR TRANSPORT (ESCRT) components LYST-INTERACTING PROTEIN 5 (LIP5) and INCREASED SALT TOLERANCE 1-LIKE1, which are involved in endosomal sorting of endocytosed plasma membrane proteins in vegetative cells (Buono et al., 2016, 2017), are required for exocytic trafficking of ABCG9, ABCG16, and other important factors required for proper pollen wall assembly (Goodman et al., 2021). The mechanisms by which both β adaptins and ESCRT proteins are redirected to the exocytic pathway in tapetal cells are currently unknown but seem to occur at intermediate stages of pollen development, after microspores are released from tetrads. In addition to investigating this switch in the regulation of trafficking pathways in tapetal cells, it will be interesting to determine whether a role of the β subunits in selecting cargo, such as ABCG9 and ABCG16, is restricted to specialized cells, such as tapetal cells, or a more general function in vegetative tissues.

In addition to the male infertility of *β1-1 β2-1/+* and *β1-2 β2-1/+* mutant plants, we also noticed partially abnormal

female gametophytic transmission of the mutant alleles. We did not investigate the endomembrane trafficking defects related to ovule or embryo sac development, but the fact that AP-1 has been previously implicated in ovule development and synergid function during pollen tube reception (Wang et al., 2016, 2017) is consistent with a similar requirement of β subunits as part of the AP-1 complex for female fertility.

Materials and methods

Bioinformatic analyses

Alignment of amino acid sequences of β adaptins was performed using DNAMAN (http://www.lynnon.com/) and protein domains were predicted by SMART (Schultz et al., 2000). A phylogenetic tree was generated using the MEGA version 6.06 software (Tamura et al., 2013).

Plant materials and growth conditions

The following transgenic lines and mutants were used in this study: *ProVHAa1:VHAa1-RFP* (Dettmer et al., 2006), *ProUBQ10:VTI12-mCherry* (provided by Dr Yiqun Bao), *ProCLC2:CLC2-mKO* (Ito et al., 2012), *ProSYP22:SYP22-RFP* (Robert et al., 2008), *Pro35S:sec-GFP* (Zheng et al., 2004), *PIN2pro:PIN2-GFP* (Xu and Scheres, 2005) transgenic lines as well as *ap1/2β1-1* (SALK_128472), *ap1/2β1-2* (SALK_002775) and *ap1/2β2-1* (SALK_150980) from the Arabidopsis Biological Resource Center mutants. Seeds from *A. thaliana* (Columbia-0) WT, single and double mutants, and transgenic plants were surface-sterilized and vernalized for 3 days at 4°C in the dark and then sown onto 1.5% (w/v) agar plates containing 1% sucrose and 0.5 × Murashige and Skoog (MS) salts. Seedlings were vertically grown on plates in a climate-controlled growth room (22°C, 16-h light/8-h dark photoperiod, and 80 $\mu Es^{-1}m^{-2}$ light intensity provided by a mixture of cool [3,000 K] and warm [6,500 K] white LED lamps), and then transplanted to soil and grown under the same light and temperature conditions.

RT-PCR and RT-qPCR

Total RNA was extracted with the RNeasy Plant Mini Kit (TIANGEN Biotech, Beijing, China). cDNAs were synthesized using reverse transcriptase according to the manufacturer's instructions (TOYOBO, Osaka, Japan) using oligo(dT) primers (TSINGKE). Transcript accumulation in mutant lines was analyzed by RT-PCR. RT-qPCRs were performed using SYBR and ROS master mixes (TOYOBO). Reactions were performed in a 20-μL volume with 10 μL of SYBR, 2 μL of ROX, 10 ng of cDNA, and 1.5 μM of specific primers with 40 cycles of 95°C for 2 min, 95°C for 3 s and 60°C for 45 s. The resulting data were analyzed with $2^{-\triangle\triangle CT}$. *ACTIN2* transcripts were used for normalization. Primer sequences are shown in Supplemental Table S6.

Generation of plasmid constructs and plant transformation

The *Proβ1/2:β1/2-GFP* and *Proβ1/2:β1/2-YFP* constructs were generated in PKGW-GWR-GFP and pBIB-GWR-YFP vectors using Gateway technology (Invitrogen, Waltham, MA, USA). The 2,007- and 2,002-bp regions upstream of the *β1* (*Proβ1*) and *β2* (*Proβ2*) coding sequences, respectively, were used to drive expression. For the GUS reporter lines, promoter regions of *β1* and *β2* were cloned into pBI121-GUS using the ScaI and XbaI, ScaI, and BamHI restriction sites. The *A9* and *ARF17* promoters were inserted into pBIB-GWR-YFP with a HindIII restriction site to make the destination vectors *ProA9:β1-YFP*, *ProA9:ABCG9-YFP*, *ProA9:ABCG16-YFP*, and *ProARF17:β1-YFP*. All constructs were transformed into Arabidopsis plants by *Agrobacterium*-mediated transformation (Clough and Bent, 1998). Sequences of primers used for cloning are listed in Supplemental Table S6.

GUS staining

Tissue staining of *Proβ1:GUS* and *Proβ2:GUS* plants was conducted as previously described (Wang et al., 2013a). Briefly, tissues of transgenic plants were incubated overnight at 37°C in a solution of 1-mg/mL X-Gluc, 10-mM EDTA (pH 8.0), 2-mM $Fe^{2+}CN$, 2-mM $Fe^{3+}CN$, 0.1% (v/v) Triton X-100 and 50-mM phosphate buffer (pH 7.0), and then washed several times in 70% ethanol until complete discoloration. Cleared tissues were mounted on microscope slides in 50% glycerol and observed using a Zeiss stereomicroscope. Floral buds were embedded in Technovit 7100 resin, sectioned into 2.5 μm slices using a Leica RM2265 microtome, and observed using a fluorescence microscope (Zeiss Axio Imager.Z2).

Self- and reciprocal crosses

The genotypes of the progeny produced by hand-pollination were analyzed by PCR to establish transmission of mutant alleles. A chi-squared test was used to establish significance of differences between the observed and expected segregation ratios. Sequences of primers used for PCR-based genotyping are listed in Supplemental Table S6.

Pollen germination and viability assays

For *in vivo* pollen tube growth, pistils from emasculated flowers were hand-pollinated. Four hours after pollination, pistils were collected and fixed for 2 h in ethanol/acetic acid (3:1), washed in double-distilled water 3 times, and incubated in 8-M NaOH solution overnight at room temperature for softening. Pistils were then washed 3 times with double-distilled water and stained with 0.1% (w/v) aniline blue staining solution (aniline blue in 0.1-M phosphate buffer, pH 11.0) for 3 h in the dark. Images were obtained using an upright fluorescence microscope (Zeiss Axio Scope A1) with UV light excitation. For the *in vitro* pollen germination assays, freshly collected pollen was smeared onto solid pollen germination medium as described previously (Zhu et al., 2017). Pollen tube length was measured using ImageJ (Schindelin et al., 2012).

Pollen viability was assessed using Alexander's staining method (Alexander, 1969) and FDA staining (Heslop-Harrison and Heslop-Harrison, 1970). Briefly, anthers collected from Stages 12 to 13 flowers were mounted on

microscope slides in a drop of Alexander's staining solution and staining solution was rinsed off with distilled water several times after 1 h incubation in a wet box at 56°C. Images were taken using a Zeiss stereomicroscope. FDA staining was performed by immersing pollen in an FDA solution (2-mg mL^{-1} FDA, 17% (w/v) sucrose, 2-mM $CaCl_2$, 1.625-mM boric acid) for 10 min. Fluorescence from living pollen grains was detected with a Zeiss Axio Scope A1 using UV excitation. At least three biological replicates were analyzed for each assay.

Histological analysis and electron microscopy imaging

Floral buds at different developmental stages were fixed in acetic acid/formaldehyde (1:3), dehydrated in a graded ethanol series, embedded in Technovit 7,100 resin, and sectioned (3-μm thick sections) using a Leica RM2265 microtome. Sections were stained with a 0.01% (w/v) toluidine blue solution before being imaged with a Zeiss Axio Imager.Z2.

For scanning electron microscopy analysis, dehiscent anthers were mounted on stubs over carbon double-sided tape and coated with gold using a sputter coater. Samples were observed in a Hitachi 4,700 scanning electron microscope.

For transmission electron microscopy analysis, floral buds were fixed with 2.5% glutaraldehyde on ice, rinsed in 0.1-M sodium phosphate-buffered saline (PBS, pH 7.0), postfixed in 2% osmium tetroxide (dissolved in 0.1-M PBS), and embedded in EPON 812 resin. Ultra-thin sections (50 nm) were double stained with 0.5% uranyl acetate and lead citrate (2.6% lead nitrate and 3.5% sodium citrate, pH 12) and observed with a transmission electron microscope (Tecnai G2 Spirit Bio-TWIN).

BiFC assays

The full-length coding sequences of *AP1γ1*, *AP1μ1*, *AP1σ2*, *AP2α1*, *AP2μ*, *AP2σ*, *AP3δ*, *AP3μ*, *AP3σ*, *AP4ε*, *AP4μ*, *AP4σ*, *ABCG9*, and *ABCG16* were cloned into the vector pEarleygate202-YC containing the C-terminal half of YFP, whereas *β1* and *β2* were cloned into the vector pEarleygate201-YN containing the N-terminal half of YFP. Pair combinations of constructs, including negative controls, were transformed into *Agrobacterium tumefaciens* strain GV3101 and cultured overnight in 5-mL of LB medium containing 50-μg mL^{-1} kanamycin and 30-μg mL^{-1} rifampin at 28°C. The bacteria were pelleted, mixed together, and infiltrated into young leaves of *N. benthamiana* plants. Randomly chosen regions of interest of infiltrated leaves were visualized by a Nikon confocal laser scanning microscope (A1R + Ti2-E) at 24–48 h after infiltration. Cells with and without YFP signal were quantified using ImageJ (Schindelin et al., 2012). Sequences of primers used for cloning are listed in Supplemental Table S6.

Co-IP and MS analysis

Liquid (0.5 × MS)-cultured 10-day-old transgenic seedlings (*Pro35S:GFP*, *Proβ1:β1-YFP* and *Proβ2:β2-YFP*) were ground in liquid nitrogen, incubated in extraction buffer (50-mM phosphate buffer [pH 7.5], 200-mM NaCl, 10-mM $MgCl_2$, 1-mM PMSF, 10% glycerol) containing a complete protease inhibitor cocktail (1 tablet/40-mL extraction buffer), and vortexed for several minutes. Extracts were centrifuged at 12,000*g* for 30 min at 4°C, and the supernatant was then incubated with 25-μL anti-GFP agarose beads (ChromoTek; 25–30 μg of recombinant GFP per 25-μL bead slurry) for 6 h at 4°C with gentle agitation. The beads were then collected and washed 45 times with extraction buffer. Protein complexes adsorbed to the beads were boiled with 2 × SDS (sodium dodecyl sulfate) loading buffer for 10 min. Proteins were separated on SDS–PAGE (sodium dodecyl sulfate–polyacrylamide gel electrophoresis) gels, stained with a 0.1% (w/v) Coomassie brilliant blue solution for 30 min, and destained in 40% methanol and 10% acetic acid until protein bands were observed. Gel strips were cut into small pieces, collected into microcentrifuge tubes, dehydrated with acetonitrile (ACN), and then incubated in 100-μL Tris (2-carboxyethyl) phosphine (10 mM, diluted with 25-mM NH_4HCO_3) for reduction at 56°C for 1 h. Centrifuge tubes were cooled-down to room temperature, and 100-μL 2-chloroacetamide (40 mM, diluted with 25-mM NH_4HCO_3) was added for alkylation in the dark for 45 min. The gel pieces were completely dehydrated by washing in 100-μL NH_4HCO_3, 50% ACN and 100% ACN 3 times, followed by drying under vacuum for 10 min.

We then added enough trypsin solution (0.01 mg mL^{-1} trypsin, diluted in 25-mM NH_4HCO_3) to cover the dry gel pieces and placed them at 4°C for 10 min for complete saturation. The tubes were then incubated in a thermostat overnight at 37°C for protein digestion. Using a microcentrifuge, we pelleted down the gel pieces, collected the supernatants in new tubes, added 100-μL extraction buffer (1:1 v/v, 5% trifluoroacetic acid/50% ACN), and incubated the samples for 15 min to extract the digested peptides. Peptide solutions were desalted using C_{18} columns, collected into tubes, and dried in a vacuum centrifuge. Finally, the tryptic peptides were redissolved in 15-μL of 0.1% formic acid (FA) for liquid chromatography (LC)–tandem MS (MS/MS) analysis.

Approximately 4-μL of peptide samples were injected into an Orbitrap Fusion Lumos MS (Thermo Fisher Scientific, Waltham, MA, USA) equipped with an EASY-nLC 1,200 system in a data-dependent mode. Briefly, samples were injected into a capillary analytic column (75-μm inner diameter) packed with C_{18} particles (2-μm diameter). The mobile phases for the LC include buffer A1 (0.1% FA) and buffer B1 (80% ACN and 0.1% FA). The peptides were separated using a 90 min nonlinear gradient consisting of buffer B1 (5%–35%) for 60 min, buffer B1 (35%–80%) for 20 min, and buffer B1 (100%) for 10 min at a constant flow rate of 300 nL min^{-1}. The electrospray voltage and current were set as 2.2 kV and 100 A, respectively. The full scan range was 100–2,000 *m/z*.

Raw MS/MS data were used to search against the *A. thaliana* Uniprot (taxonomy 3,702) database (52,619 total entries). Protein annotations, identification, and spectral area-based LFQ were done with Proteomics Discovery 2.2 software (Thermo Fisher Scientific). Peptide mass tolerance was set at 15 ppm. The output data contain input group samples and co-IP samples immunoprecipitated by GFP beads from three biological replicates. All data (including LFQ data) were filtered by 1% false discovery rate to identify high confidence proteins with at least one unique peptide. Specific proteins for the β1-YFP and β2-YFP co-IPs were determined in three steps: (1) proteins with co-IP/input ratio significantly enriched ($P < 0.05$); (2) union of three biological replicates from Step 1 for 35S-GFP; and intersection of three biological replicates from Step 1 for β1/2-YFP; (3) union of pairwise intersection of three biological replicates in co-IP groups by identifying significantly enriched proteins based on β1/2-YFP/35S-GFP ratio ($P < 0.05$).

Y2H assays

Interactions between β1/2 and ABCG9/16 were analyzed using a mbSUS (Obrdlik et al., 2004). Full-length coding regions of *ABCG9*, *ABCG16*, *β1*, and *β2* were amplified by PCR, cloned into pMetYCgate or pX-NubWTgate vectors, and transformed into yeast strains THY.AP4 or THY.AP5. Transformants were selected on a synthetic complete medium containing adenine and histidine. Interactions were detected by growing yeast cells on a synthetic minimal medium supplied with different concentrations of methionine. Empty pMetYC and pX-NubWT vectors were used as negative controls. The sequences of primers used for cloning are listed in Supplemental Table S6.

Confocal laser scanning microscopy

All confocal images were captured using a Nikon laser scanning confocal microscope (A1R + Ti2-E) with a 40 × water-immersion objective (NA = 1.25). GFP and YFP were excited with a 488 nm argon laser line and the emission was collected between 500 and 550 nm. RFP, mKO, mCherry, and FM4–64 were excited with a 561 nm argon laser line and the emission was collected between 570 and 620 nm. Chlorophyll was excited with a 640-nm argon laser line and its emission was collected between 663 and 738 nm. Pollen wall autofluorescence was visualized by excitation at 405 nm and emission was collection between 425 and 475 nm. Images were quantified with ImageJ (Schindelin et al., 2012). The Colocalization Finder plugin of ImageJ was used to calculate the Pearson's correlation coefficients and Spearman's rank correlation coefficients.

Pharmacological treatments

Dimethyl sulfoxide was used to prepare stock solutions of CHX (100-mM), BFA (100-mM), and FM4–64 (2-mM). Final working concentrations were diluted in 0.5 × MS liquid. Five-day-old seedlings were used for analysis of root cell trafficking defects using 50-μM CHX, 50-μM BFA, and 2-μM FM4–64. Incubation times are indicated in the text and figures. Developing anthers were dissected from floral buds and incubated in BFA for 2 h or pretreated with 100-μM CHX for 30 min, and then incubated with 100-μM BFA plus 100-μM CHX for 2 h.

Statistical analysis

Statistical analyses were performed in Microsoft Excel unless otherwise stated. One-way analysis of variance (ANOVA) used for multiple comparisons with a post-hoc Tukey test was conducted using the online calculator astatsa.com. ANOVA and *t* test tables are included in Supplemental File S1.

Accession numbers

The sequences data mentioned in this article can be found in the Arabidopsis Information Resource (https://www.arabidopsis.org/) using the following accession numbers: *AP1/2β1* (At4g11380), *AP1/2β2* (At4g23460), *AP1γ1* (At1g60070), *AP1μ1* (At1g10730), *AP1σ2* (AT2g17380), *AP2α1* (At5g22770), *AP2μ* (At5g46630), *AP2σ* (At1g47830), *AP3δ* (AT1g48760), *AP3μ* (At1g56590), *AP3σ* (At3g50860), *AP4ε* (At1g31730), *AP4μ* (AT4g24550), *AP4σ* (At2g19790), *ABCG9* (At4g27420), *ABCG16* (At3g55090), *A9* (At5g07230), *ARF17* (At1g77850), and *ACTIN2* (At3g18780). The MS proteomics data have been deposited to the ProteomeXchange Consortium via the PRIDE partner repository (https://www.ebi.ac.uk/pride/) with the dataset identifier PXD031514.

Supplemental data

The following materials are available in the online version of this article.

Supplemental Figure S1. Analysis of AP1/2β amino acid sequences in different species.

Supplemental Figure S2. BiFC interaction assay.

Supplemental Figure S3. Expression patterns of Arabidopsis β1 and β2 adaptins.

Supplemental Figure S4. Colocalization analysis of β2 with TGN and vacuolar markers in tapetum and pollen grains.

Supplemental Figure S5. Phenotypic characterization of β1 and β2 loss-of-function mutants.

Supplemental Figure S6. Phenotypic characterization of single and double *β1* and *β2* mutants.

Supplemental Figure S7. Rescue of mutant phenotypic defects by expression of β1-GFP and β2-GFP.

Supplemental Table S1. Proteins co-immunoprecipitated with β1-YFP.

Supplemental Table S2. Proteins co-immunoprecipitated with β2-YFP.

Supplemental Table S3. GO term (biological processes) enrichment analysis for proteins co-immunoprecipitated with β1-YFP.

Supplemental Table S4. GO term (biological processes) enrichment analysis for proteins co-immunoprecipitated with β2-YFP.

Supplemental Table S5. Statistical analysis of offspring genotype segregation ratio from self and reciprocal crosses of $\beta 1$ $\beta 2$ double mutants.

Supplemental Table S6. Primer sequences used in this study.

Supplemental Data Set 1. Alignments used to generate the phylogeny presented in Supplemental Figure S1B.

Supplemental File S1. ANOVA and *t* test Tables.

Acknowledgments

We thank Dr Yiqun Bao (College of Life Sciences, Nanjing Agricultural University) for providing seeds of *ProUBQ10:VTI12-mCherry* line, Dr Xiaoping Gou (School of Life Sciences, Lanzhou University) for providing the vectors pBIB-GWR-YFP, pEarleygate201-YN and pEarleygate202-YC, pMetYCgate and pX-NubWTgate; Drs Sebastian Y. Bednarek (Department of Biochemistry, University of Wisconsin-Madison) and Xiaofeng Xu (College of Life Sciences, Shanghai Normal University) for valuable suggestions on this research project. We are grateful to Dr Yahu Gao, Liang Peng, Dr Yang Zhao, Liping Guan, Haiyan Li, and Xia Deng (Core Facility for Life Science Research, Lanzhou University) for their technical assistance.

Funding

This work was funded by the National Natural Science Foundation of China (grants 31820103008 and 91754104 to J.P.), the Youth Program of National Natural Science Foundation of China (grant 31801193 to C.W.), the Startup Foundation for Introducing Talent of Lanzhou University (grant 561120206 to H.W.), and the U.S. National Foundation (MCB grant 2114603 to M.S.O).

Conflict of interest statement. The authors declare no conflict of interest.

References

Aboulela M, Nakagawa T, Oshima A, Nishimura K, Tanaka Y (2018) The Arabidopsis COPII components, AtSEC23A and AtSEC23D, are essential for pollen wall development and exine patterning. J Exp Bot **69**: 1615–1633

Alexander MP (1969) Differential staining of aborted and nonaborted pollen. Stain Technol **44**: 117–122

Ariizumi T, Toriyama K (2011) Genetic regulation of sporopollenin synthesis and pollen exine development. Annu Rev Plant Biol **62**: 437–460

Bassham DC, Brandizzi F, Otegui MS, Sanderfoot AA (2008) The secretory system of Arabidopsis. Arabidopsis Book **6**: e0116

Blackmore S, Wortley AH, Skvarla JJ, Rowley JR (2007) Pollen wall development in flowering plants. New Phytol **174**: 483–498

Boehm M, Bonifacino JS (2001) Adaptins: the final recount. Mol Biol Cell **12**: 2907–2920

Buono RA, Paez-Valencia J, Miller ND, Goodman K, Spitzer C, Spalding EP, Otegui MS (2016) Role of SKD1 regulators LIP5 and IST1-LIKE1 in endosomal sorting and plant development. Plant Physiol **171**: 251–264

Buono RA, Leier A, Paez-Valencia J, Pennington J, Goodman K, Miller N, Ahlquist P, Marquez-Lago T, Otegui MS (2017) ESCRT-mediated vesicle concatenation in plant endosomes. J. Cell Biol **216**: 2167–2177

Chen Z, Schmid SL (2020) Evolving models for assembling and shaping clathrin-coated pits. J Cell Biol **219**: e202005126

Choi H, Jin JY, Choi S, Hwang JU, Kim YY, Suh MC, Lee Y (2011) An ABCG/WBC-type ABC transporter is essential for transport of sporopollenin precursors for exine formation in developing pollen. Plant J **65**: 181–193

Choi H, Ohyama K, Kim YY, Jin JY, Lee SB, Yamaoka Y, Muranaka T, Suh MC, Fujioka S, Lee Y (2014) The role of Arabidopsis ABCG9 and ABCG31 ATP binding cassette transporters in pollen fitness and the deposition of steryl glycosides on the pollen coat. Plant Cell **26**: 310–324

Clough S, Bent A (1998) Floral dip: a simplified method for *Agrobacterium* -mediated transformation of *Arabidopsis thaliana*. Plant J **16**: 735–743

Dacks JB, Poon PP, Field MC (2008) Phylogeny of endocytic components yields insight into the process of nonendosymbiotic organelle evolution. Proc Natl Acad Sci USA **105**: 588–593

Dettmer J, Hong-Hermesdorf A, Stierhof YD, Schumacher K (2006) Vacuolar H^+-ATPase activity is required for endocytic and secretory trafficking in *Arabidopsis*. Plant Cell **18**: 715–730

Di Rubbo S, Irani NG, Kim SY, Xu ZY, Gadeyne A, Dejonghe W, Vanhoutte I, Persiau G, Eeckhout D, Simon S, et al (2013) The clathrin adaptor complex AP-2 mediates endocytosis of BRASSINOSTEROID INSENSITIVE1 in *Arabidopsis*. Plant Cell **25**: 2986–2997

Doray B, Lee I, Knisely J, Bu G, Kornfeld S (2007) The gamma/-sigma1 and alpha/sigma2 hemicomplexes of clathrin adaptors AP-1 and AP-2 harbor the dileucine recognition site. Mol Biol Cell **18**: 1887–1896

Dou XY, Yang KZ, Zhang Y, Wang W, Liu XL, Chen LQ, Zhang XQ, Ye D (2011) WBC27, an adenosine tri-phosphate-binding cassette protein, controls pollen wall formation and patterning in *Arabidopsis*. J Integr Plant Biol **53**: 74–88

Fan L, Hao H, Xue Y, Zhang L, Song K, Ding Z, Botella MA, Wang H, Lin J (2013) Dynamic analysis of Arabidopsis AP2 sigma subunit reveals a key role in clathrin-mediated endocytosis and plant development. Development **140**: 3826–3837

Fan X, Yang C, Klisch D, Ferguson A, Bhaellero RP, Niu X, Wilson ZA (2014) ECHIDNA protein impacts on male fertility in Arabidopsis by mediating trans-Golgi network secretory trafficking during anther and pollen development. Plant Physiol **164**: 1338–1349

Feng C, Wang JG, Liu HH, Li S, Zhang Y (2017) Arabidopsis adaptor protein 1G is critical for pollen development. J Integr Plant Biol **59**: 594–599

Goodman K, Paez Valencia J, Pennington J, Sonntag A, Ding X, Lee HN, Ahlquist P, Molina I, Otegui MS (2021) ESCRT components ISTL1 and LIP5 are required for tapetal function and pollen viability Plant Cell **33**: 2850–2868

Happel N, Honing S, Neuhaus JM, Paris N, Robinson DG, Holstein SEH (2004) *Arabidopsis* mu A-adaptin interacts with the tyrosine motif of the vacuolar sorting receptor VSR-PS1. Plant J **37**: 678–693

Heinze L, Freimuth N, Rößling AK, Hahnke R, Riebschläger S, Fröhlich A, Sampathkumar A, McFarlane HE, Sauer M (2020) EPSIN1 and MTV1 define functionally overlapping but molecularly distinct trans-Golgi network subdomains in Arabidopsis. Proc Natl Acad Sci USA **117**: 25880–25889

Heslop-Harrison J, Heslop-Harrison Y (1970) Evaluation of pollen viability by enzymatically induced fluorescence; intracellular hydrolysis of fluorescein diacetate. Stain Technol **45**: 115–120

Ito E, Fujimoto M, Ebine K, Uemura T, Ueda T, Nakano A (2012) Dynamic behavior of clathrin in *Arabidopsis thaliana* unveiled by live imaging. Plant J **69**: 204–216

Janvier K, Kato Y, Boehm M, Rose JR, Martina JA, Kim BY, Venkatesan S, Bonifacino JS (2003) Recognition of

dileucine-based sorting signals from HIV-1 Nef and LIMP-II by the AP-1 gamma-sigma1 and AP-3 delta-sigma3 hemicomplexes. J Cell Biol **163**: 1281–1290

Kelly BT, Graham SC, Liska N, Dannhauser PN, Höning S, Ungewickell EJ, Owen DJ (2014) Clathrin adaptors. AP2 controls clathrin polymerization with a membrane-activated switch. Science **345**: 459–463

Keyel PA, Thieman JR, Roth R, Erkan E, Everett ET, Watkins SC, Heuser JE, Traub LM (2008) The AP-2 adaptor beta2 appendage scaffolds alternate cargo endocytosis. Mol Biol Cell **19**: 5309–5326

Kim SY, Xu ZY, Song K, Kim DH, Kang H, Reichardt I, Sohn EJ, Friml J, Juergens G, Hwang I (2013) Adaptor protein complex 2-mediated endocytosis is crucial for male reproductive organ development in Arabidopsis. Plant Cell **25**: 2970–2985

Kovtun O, Dickson VK, Kelly BT, Owen DJ, Briggs JG (2020) Architecture of the AP2/clathrin coat on the membranes of clathrin-coated vesicles. Sci Adv **6**: eaba8381

Kuromori T, Ito T, Sugimoto E, Shinozaki K (2011) *Arabidopsis* mutant of AtABCG26, an ABC transporter gene, is defective in pollen maturation. J Plant Physiol **168**: 2001–2005

Lee I, Doray B, Govero J, Kornfeld S (2008) Binding of cargo sorting signals to AP-1 enhances its association with ADP ribosylation factor 1-GTP. J Cell Biol **180**: 467–472

Liang X, Li SW, Gong LM, Li S, Zhang Y (2020) COPII components Sar1b and Sar1c play distinct yet interchangeable roles in pollen development. Plant Physiol **183**: 974–985

Liu D, Kumar R, Claus LAN, Johnson AJ, Siao W, Vanhoutte I, Wang P, Bender KW, Yperman K, Martins S, et al (2020) Endocytosis of BRASSINOSTEROID INSENSITIVE1 Is partly driven by a canonical Tyr-based motif. Plant Cell **32**: 3598–3612

Martzoukou O, Amillis S, Zervakou A, Christoforidis S, Diallinas G (2017) The AP-2 complex has a specialized clathrin-independent role in apical endocytosis and polar growth in fungi. eLife **6**: e20083

Mehrani A, Stagg SM (2022) Probing intracellular vesicle trafficking and membrane remodelling by cryo-EM. J Struct Biol **214**: 107836

Mishra SK, Hawryluk MJ, Brett TJ, Keyel PA, Dupin AL, Jha A, Heuser JE, Fremont DH, Traub LM (2004) Dual engagement regulation of protein interactions with the AP-2 adaptor alpha appendage. J Biol Chem **279**: 46191–46203

Obrdlik P, El-Bakkoury M, Hamacher T, Cappellaro C, Vilarino C, Fleischer C, Ellerbrok H, Kamuzinzi R, Ledent V, Blaudez D, et al (2004) K + channel interactions detected by a genetic system optimized for systematic studies of membrane protein interactions. Proc Natl Acad Sci USA **101**: 12242–12247

Ohno H, Fournier MC, Poy G, Bonifacino JS (1996) Structural determinants of interaction of tyrosine-based sorting signals with the adaptor medium chains. J Biol Chem **271**: 29009–29015

Ohno H, Aguilar RC, Yeh D, Taura D, Saito T, Bonifacino JS (1998) The medium subunits of adaptor complexes recognize distinct but overlapping sets of tyrosine-based sorting signals. J Biol Chem **273**: 25915–25921

Ohno H, Stewart J, Fournier MC, Bosshart H, Rhee I, Miyatake S, Saito T, Gallusser A, Kirchhausen T, Bonifacino JS (1995) Interaction of tyrosine-based sorting signals with clathrin-associated proteins. Science **269**: 1872–1875

Paraan M, Mendez J, Sharum S, Kurtin D, He H, Stagg SM (2020) The structures of natively assembled clathrin-coated vesicles. Sci Adv **6**: eaba8397

Park M, Song K, Reichardt I, Kim H, Mayer U, Stierhof YD, Hwang I, Jürgens G (2013) Arabidopsis μ-adaptin subunit AP1M of adaptor protein complex 1 mediates late secretory and vacuolar traffic and is required for growth. Proc Natl Acad Sci USA **110**: 10318–10323

Park Y, Xu ZY, Kim SY, Lee J, Choi B, Lee J, Kim H, Sim HJ, Hwang I (2016) Spatial regulation of ABCG25, an ABA exporter, is an important component of the mechanism controlling cellular ABA levels. Plant Cell **28**: 2528–2544

Paul W, Hodge R, Smartt S, Draper J, Scott R (1992) The isolation and characterisation of the tapetum-specific *Arabidopsis thaliana* A9 gene. Plant Mol Biol **19**: 611–622

Quilichini TD, Samuels AL, Douglas CJ (2014) ABCG26-mediated polyketide trafficking and hydroxycinnamoyl spermidines contribute to pollen wall exine formation in *Arabidopsis*. Plant Cell **26**: 4483–4498

Quilichini TD, Friedmann MC, Samuels AL, Douglas CJ (2010) ATP-binding cassette transporter G26 is required for male fertility and pollen exine formation in *Arabidopsis*. Plant Physiol **154**: 678–690

Rapoport I, Chen YC, Cupers P, Shoelson SE, Kirchhausen T (1998) Dileucine-based sorting signals bind to the beta chain of AP-1 at a site distinct and regulated differently from the tyrosine-based motif-binding site. EMBO J **17**: 2148–2155

Robert S, Chary SN, Drakakaki G, Li S, Yang Z, Raikhel NV, Hicks GR (2008) Endosidin1 defines a compartment involved in endocytosis of the brassinosteroid receptor BRI1 and the auxin transporters PIN2 and AUX1. Proc Natl Acad Sci USA **105**: 8464–8469

Rosa P, Barr FA, Stinchcombe JC, Binacchi C, Huttner WB (1992) Brefeldin A inhibits the formation of constitutive secretory vesicles and immature secretory granules from the trans-Golgi network. Eur J Cell Biol **59**: 265–274

Sanders PM, Bui AQ, Weterings K, McIntire KN, Hsu YC, Lee PY, Truong MT, Beals TP, Goldberg RB (1999) Anther developmental defects in *Arabidopsis thaliana* male-sterile mutants. Sex Plant Reprod **11**: 297–322

Schindelin J, Arganda-Carreras I, Frise E, Kaynig V, Longair M, Pietzsch T, Preibisch S, Rueden C, Saalfeld S, Schmid B, et al (2012) Fiji: an open-source platform for biological-image analysis. Nat Methods **9**: 676–682

Schultz J, Copley RR, Doerks T, Ponting CP, Bork P (2000) SMART: a web-based tool for the study of genetically mobile domains. Nucleic Acids Res **28**: 231–234

Shih W, Gallusser A, Kirchhausen T (1995) A clathrin-binding site in the hinge of the beta 2 chain of mammalian AP-2 complexes. J Biol Chem **270**: 31083–31090

Shimada T, Kunieda T, Sumi S, Koumoto Y, Tamura K, Hatano K, Ueda H, Hara-Nishimura I (2018) The AP-1 complex is required for proper mucilage formation in *Arabidopsis* seeds. Plant Cell Physiol **59**: 2331–2338

Shimizu Y, Takagi J, Ito E, Ito Y, Ebine K, Komatsu Y, Goto Y, Sato M, Toyooka K, Ueda T, et al (2021) Cargo sorting zones in the trans-Golgi network visualized by super-resolution confocal live imaging microscopy in plants. Nat Commun **12**: 1901–1901

Smith SM, Larocque G, Wood KM, Morris KL, Roseman AM, Sessions RB, Royle SJ, Smith CJ (2021) Multi-modal adaptor-clathrin contacts drive coated vesicle assembly. EMBO J **40**: e108795–e108795

Smyth DR, Bowman JL, Meyerowitz EM (1990) Early flower development in Arabidopsis. Plant Cell **2**: 755

Tamura K, Stecher G, Peterson D, Filipski A, Kumar S (2013) MEGA6: molecular evolutionary genetics analysis version 6.0. Mol Biol Evol **30**: 2725–2729

Teh OK, Shimono Y, Shirakawa M, Fukao Y, Tamura K, Shimada T, Hara-Nishimura I (2013) The AP-1 μ adaptin is required for KNOLLE localization at the cell plate to mediate cytokinesis in Arabidopsis. Plant Cell Physiol **54**: 838–847

Tse YC, Lo SW, Hillmer S, Dupree P, Jiang L (2006) Dynamic response of prevacuolar compartments to brefeldin a in plant cells. Plant Physiol **142**: 1442–1459

Wang C, Yan X, Chen Q, Jiang N, Fu W, Ma B, Liu J, Li C, Bednarek SY, Pan J (2013a) Clathrin light chains regulate clathrin-mediated trafficking, auxin signaling, and development in Arabidopsis. Plant Cell **25**: 499–516

Wang JG, Li S, Zhao XY, Zhou LZ, Huang GQ, Feng C, Zhang Y (2013b) HAPLESS13, the *Arabidopsis* μ1 adaptin, is essential for protein sorting at the trans-Golgi network/early endosome. Plant Physiol **162**: 1897–1910

Wang JG, Feng C, Liu HH, Feng QN, Li S, Zhang Y (2017) AP1G mediates vacuolar acidification during synergid-controlled pollen tube reception. Proc Natl Acad Sci USA **114**: e4877–e4883

Wang JG, Feng C, Liu HH, Ge FR, Li S, Li HJ, Zhang Y (2016) HAPLESS13-mediated trafficking of STRUBBELIG is critical for ovule development in *Arabidopsis*. PLoS Genet **12**: e1006269

Wang LH, Südhof TC, Anderson RG (1995) The appendage domain of alpha-adaptin is a high affinity binding site for dynamin. J Biol Chem **270**: 10079–10083

Wang X, Cai Y, Wang H, Zeng Y, Zhuang X, Li B, Jiang L (2014) Trans-Golgi network-located AP1 gamma adaptins mediate dileucine motif-directed vacuolar targeting in Arabidopsis. Plant Cell **26**: 4102–4118

Xu J, Scheres B (2005) Dissection of Arabidopsis ADP-RIBOSYLATION FACTOR 1 function in epidermal cell polarity. Plant Cell **17**: 525–536

Xu M, Yan X, Wang Y, Liu C, Yang Q, Tian D, Bednarek SY, Pan J, Wang C (2022) ADAPTOR PROTEIN-1 complex-mediated post-Golgi trafficking is critical for pollen wall development in Arabidopsis. New Phytol **235**: 472–487

Yamaoka S, Shimono Y, Shirakawa M, Fukao Y, Kawase T, Hatsugai N, Tamura K, Shimada T, Hara-Nishimura I (2013) Identification and dynamics of Arabidopsis adaptor protein-2 complex and its involvement in floral organ development. Plant Cell **25**: 2958–2969

Yan X, Wang Y, Xu M, Dahhan DA, Liu C, Zhang Y, Lin J, Bednarek SY, Pan J (2021) Cross-talk between clathrin-dependent post-Golgi trafficking and clathrin-mediated endocytosis in Arabidopsis root cells. Plant Cell **33**: 3057–3075

Yang J, Tian L, Sun MX, Huang XY, Zhu J, Guan YF, Jia QS, Yang ZN (2013) AUXIN RESPONSE FACTOR17 is essential for pollen wall pattern formation in Arabidopsis. Plant Physiol **162**: 720–731

Yim S, Khare D, Kang J, Hwang JU, Liang W, Martinoia E, Zhang D, Kang B, Lee Y (2016) Postmeiotic development of pollen surface layers requires two *Arabidopsis* ABCG-type transporters. Plant Cell Rep **35**: 1863–1873

Yoshinari A, Hosokawa T, Amano T, Beier MP, Kunieda T, Shimada T, Hara-Nishimura I, Naito S, Takano J (2019) Polar localization of the borate exporter BOR1 requires AP2-dependent endocytosis. Plant Physiol **179**: 1569–1580

Zhao B, Shi H, Wang W, Liu X, Gao H, Wang X, Zhang Y, Yang M, Li R, Guo Y (2016) Secretory COPII protein SEC31B is required for pollen wall development. Plant Physiol **172**: 1625–1642

Zheng H, Kunst L, Hawes C, Moore I (2004) A GFP-based assay reveals a role for RHD3 in transport between the endoplasmic reticulum and Golgi apparatus. Plant J **37**: 398–414

Zhu J, Nan Q, Qin T, Qian D, Mao T, Yuan S, Wu X, Niu Y, Bai Q, An L, et al (2017) Higher-ordered actin structures remodeled by *Arabidopsis* ACTIN-DEPOLYMERIZING FACTOR5 are important for pollen germination and pollen tube growth. Mol Plant **10**: 1065–1081